AD-A122 150 THE DETERMINATION OF THE APERTURE DISTRIBUTION OF A LINEAR ARRAY THROUGH..(U) OHIO STATE UNIV COLUMBUS ELECTROSCIENCE LAB R F BACKHUS JUN 82 ESL-713303-2 2/2

UNCLASSIFIED N62269-80-C-0384 F/G 20/14 NL

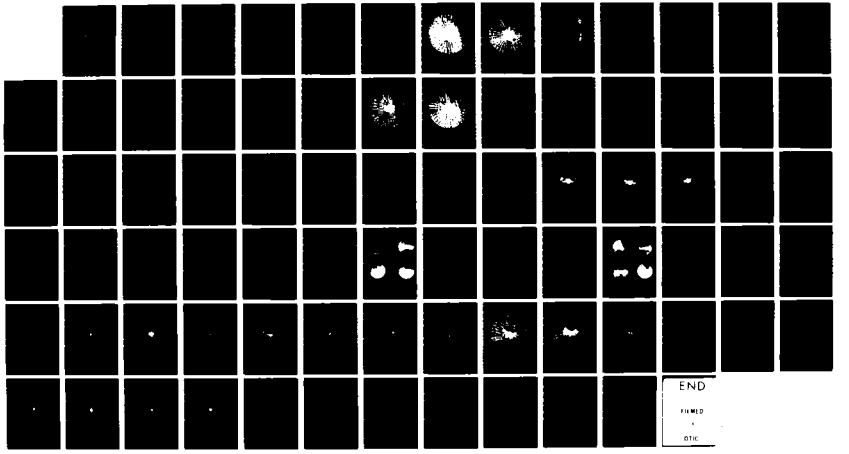

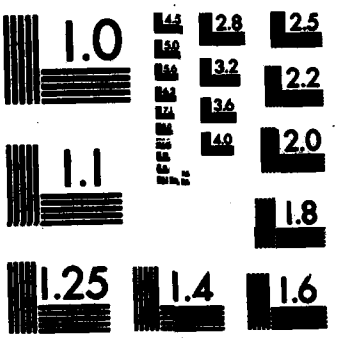

TABLE 9

UNCONSTRAINED ARRAY CURRENTS FOR y=15.8 cm MEASUREMENTS ALONG WITH SOURCE NORM, PATTERN ERROR, AND QUALITY NUMBER

ARRAY ELEMENT #	CURRENT MAGNITUDE	CURRENT PHASE
1	0.00137	1.659
2	0.0219	-29.90
3	0.120	-180.0
4	0.116	-75.79
5	0.253	-167.7
6	0.395	-29.76
7	0.466	-180.3
8	0.692	-11.61
8	0.746	166.0
10	1.00	-12.00
11	0.849	170.3
12	0.928	-2.120
13	0.755	163.8
14	0.558	6.963
15	0.446	172.2
16	0.173	19.53
17	0.287	-177.8
18	0.0565	-133.9
19	0.0329	172.3
20	0.0133	-4.283
$\|f'\|=7.74\times10^{-3}$	$E=7.93\times10^{-4}$	$Q=3.17\times10^{-4}$

TABLE 10

CONSTRAINED ARRAY CURRENTS FOR y=15.8 cm MEASUREMENTS
ALONG WITH SOURCE NORM, PATTERN ERROR,
AND QUALITY NUMBER

ARRAY ELEMENT #	CURRENT MAGNITUDE	CURRENT PHASE
1	0.0483	-5.281
2	0.0769	-121.4
3	0.392	-180.0
4	1.00	-142.8
5	0.618	-100.5
6	0.949	-107.4
7	0.752	-64.99
8	0.111	-50.32
9	0.479	19.50
10	0.888	-26.96
11	0.252	-17.91
12	0.965	35.46
13	0.856	88.47
14	0.831	95.36
15	0.331	108.8
16	0.888	149.8
17	0.873	174.0
18	0.899	-161.0
19	0.0854	97.03
20	0.0496	-36.31
$\|f'\|=1.45\times10^{-3}$,	$E=8.02\times10^{-4}$,	$Q=1.11\times10^{-5}$

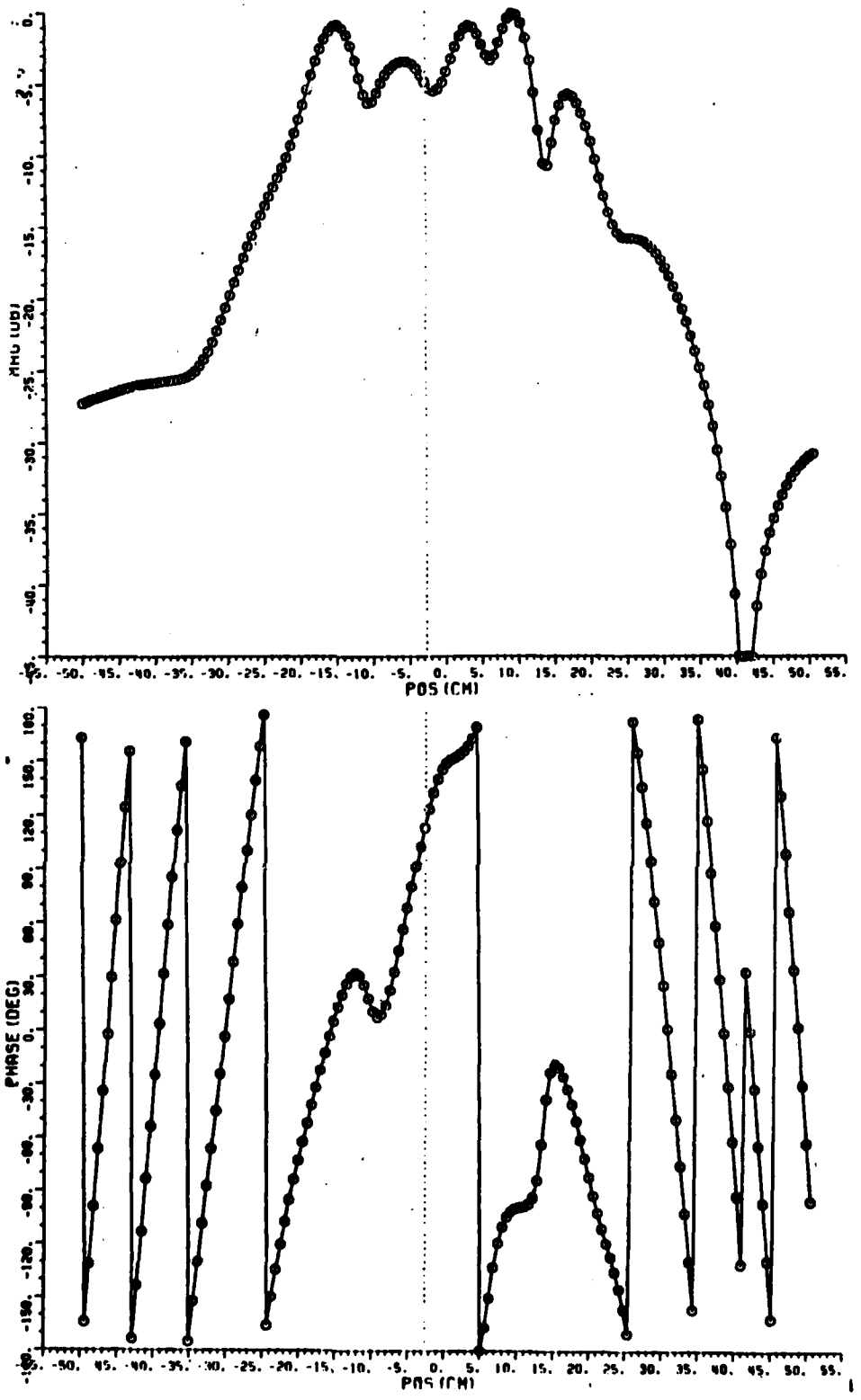

Figure 45: Computed near field for constrained currents from y=15.8 cm measurement data.

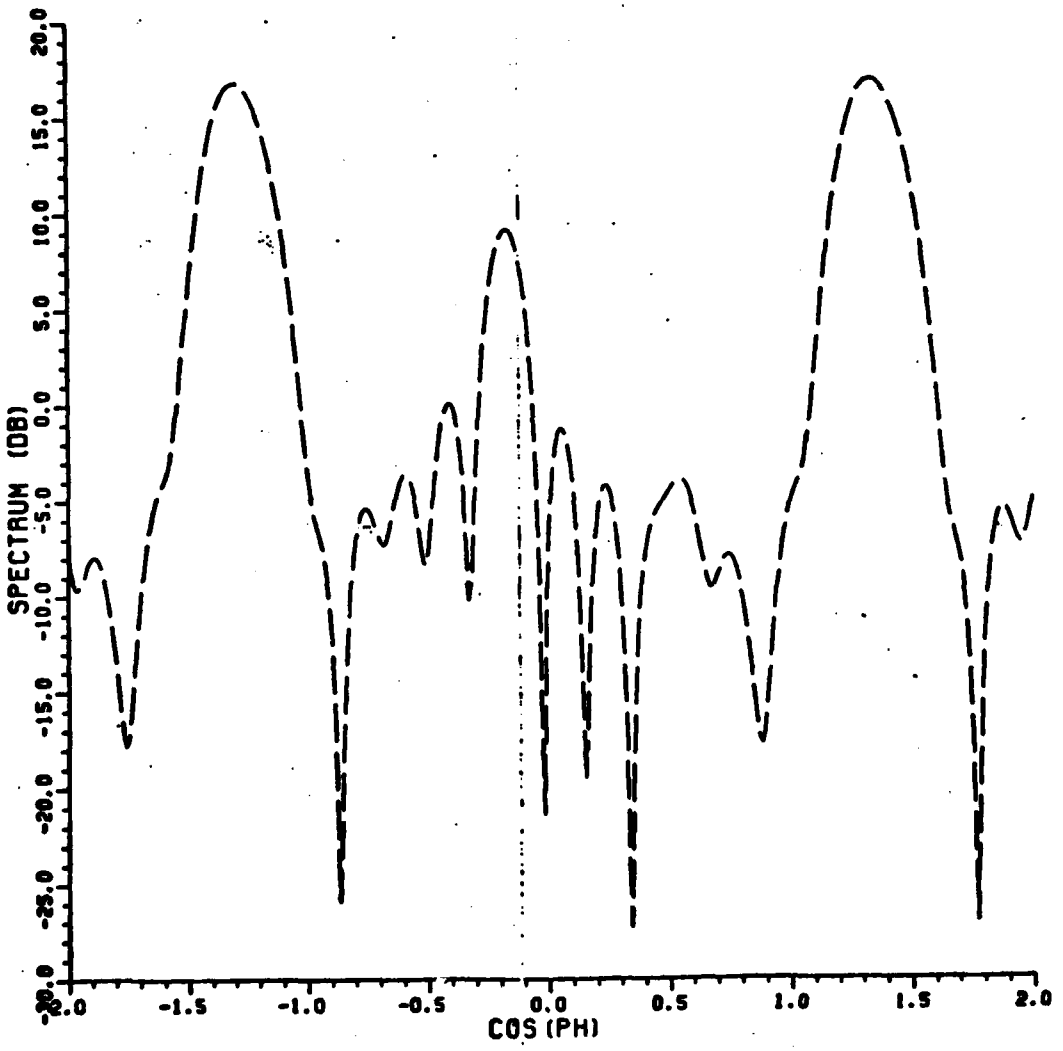

Figure 46: Free space spectrum for unconstrained array currents (y=15.8 cm).

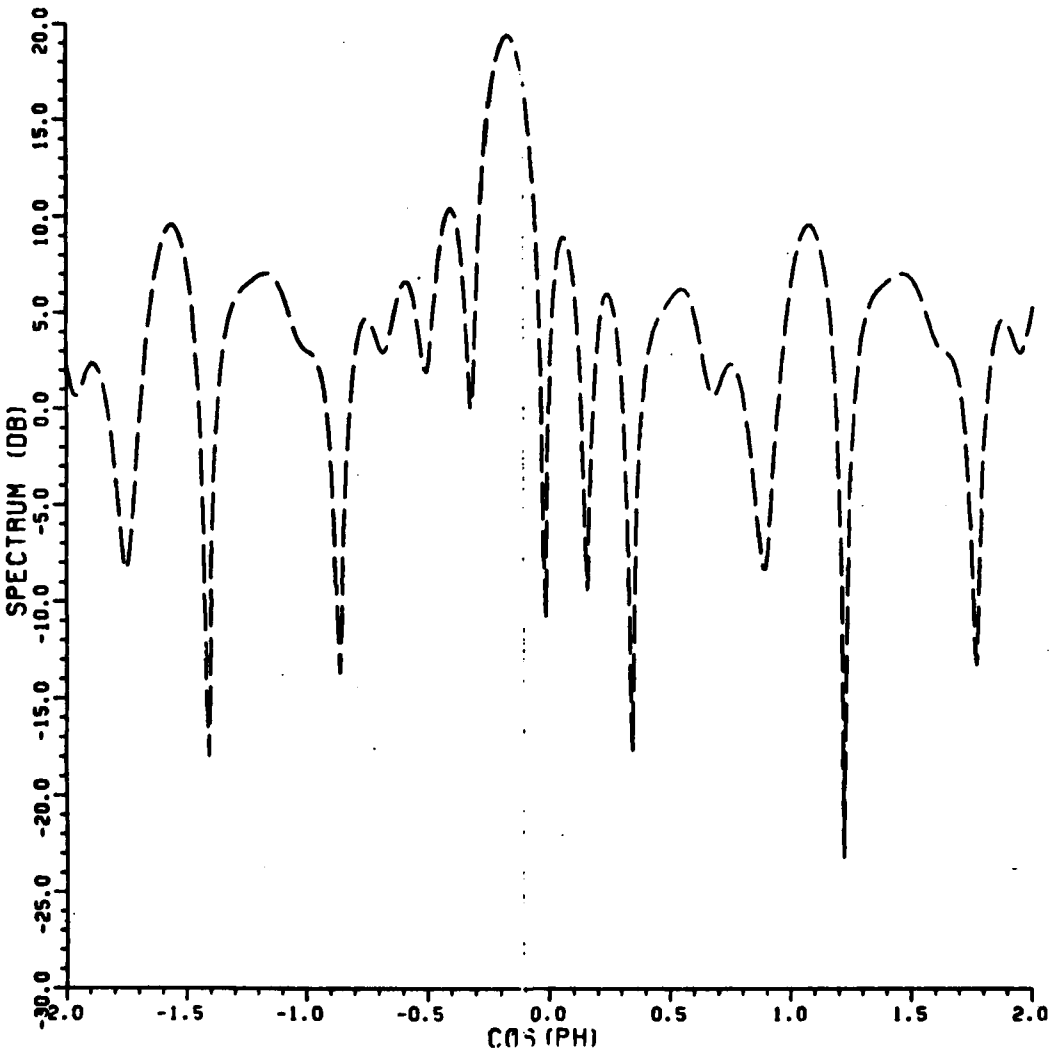

Figure 47: Free space spectrum for constrained array currents (y=15.8 cm).

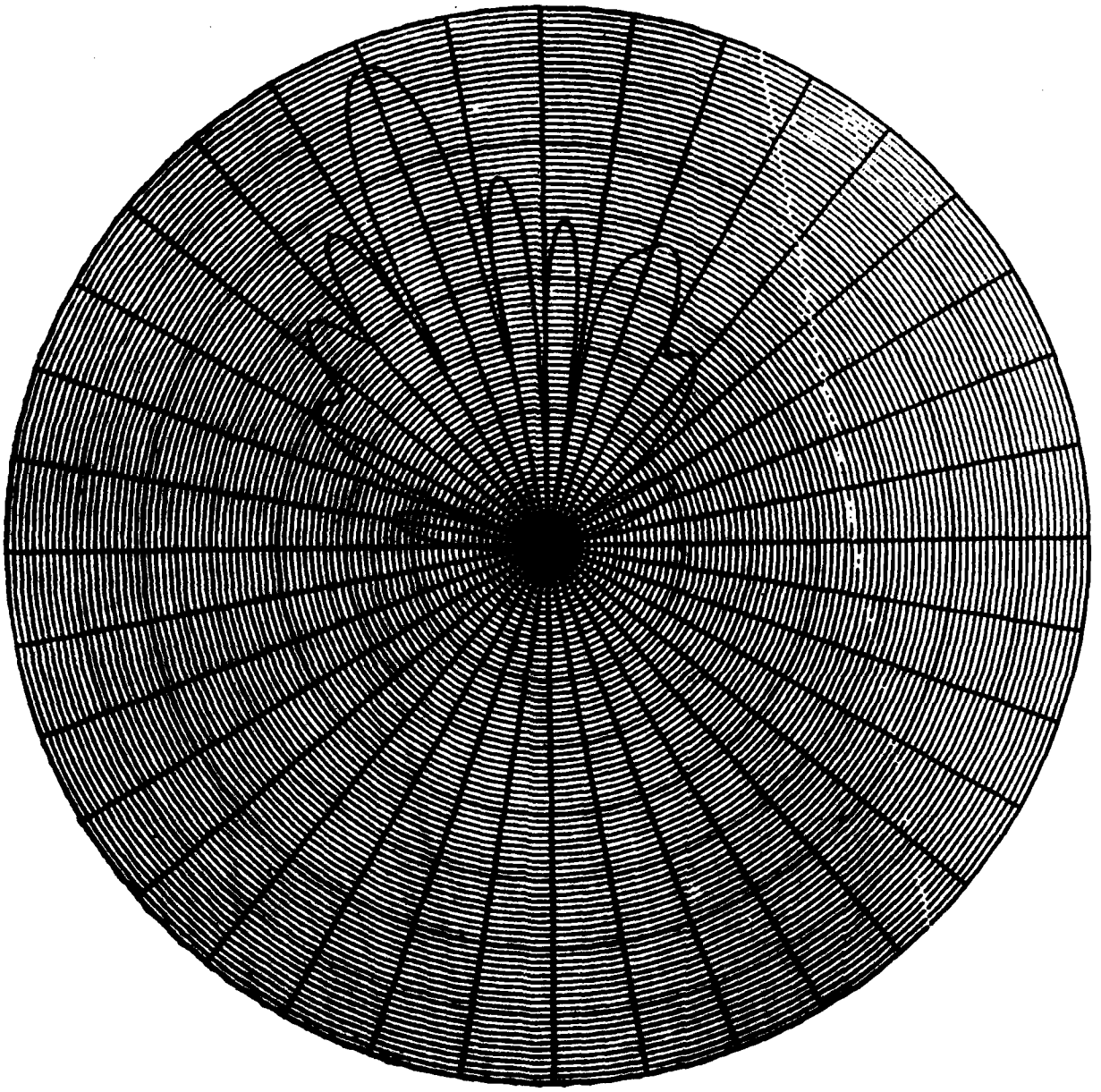

Figure 48: Computed fresnel region pattern of array for the constrained currents corresponding to y=15.8 cm near field measurements.

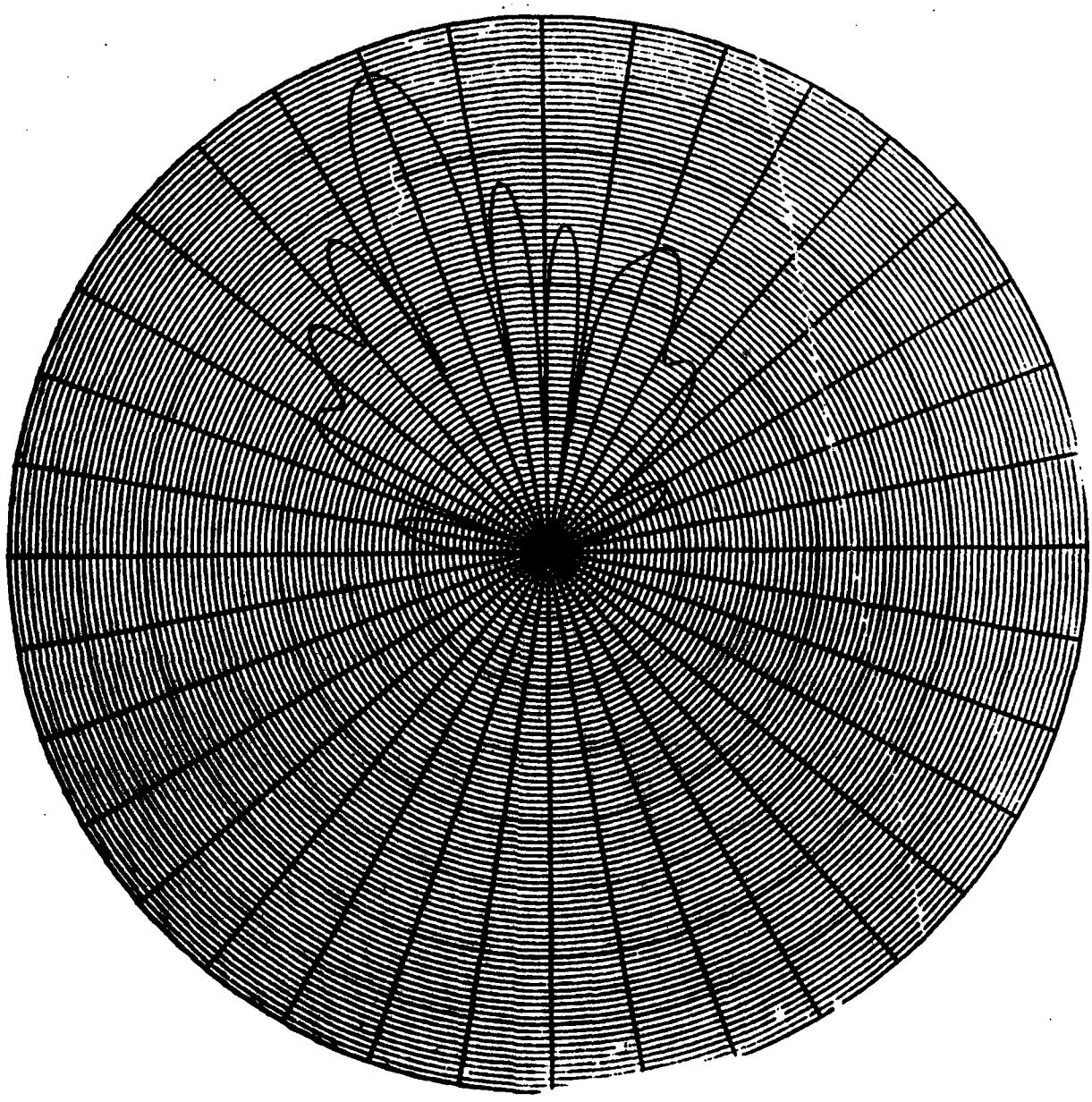

Figure 49: Computed fresnel region pattern of array for the unconstrained currents corresponding to y=15.8 cm near field measurements.

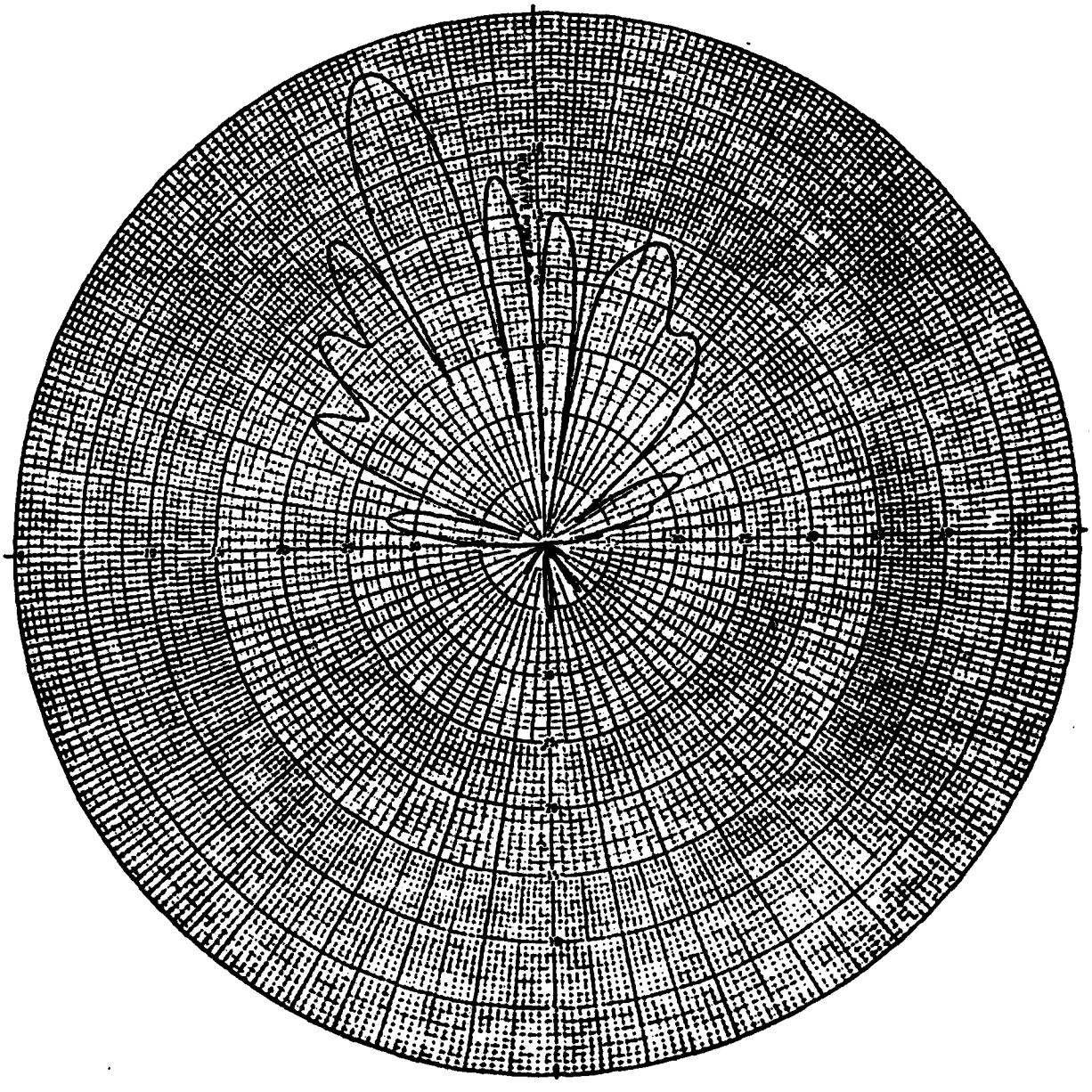

Figure 50: Measured fresnel region pattern of array at a radial distance of 10 m.

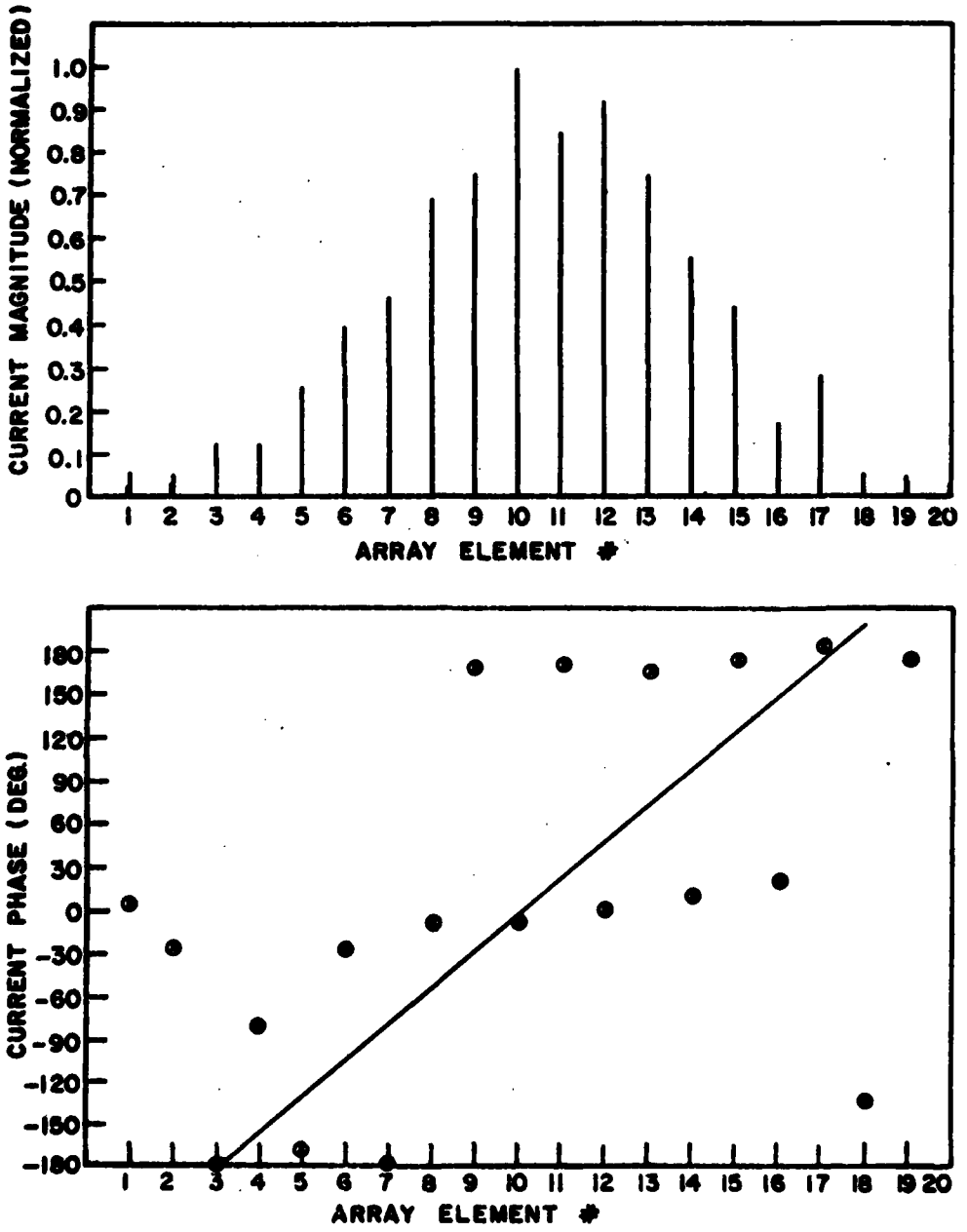

Figure 51: Unconstrained array current plots (y=15.8 cm).

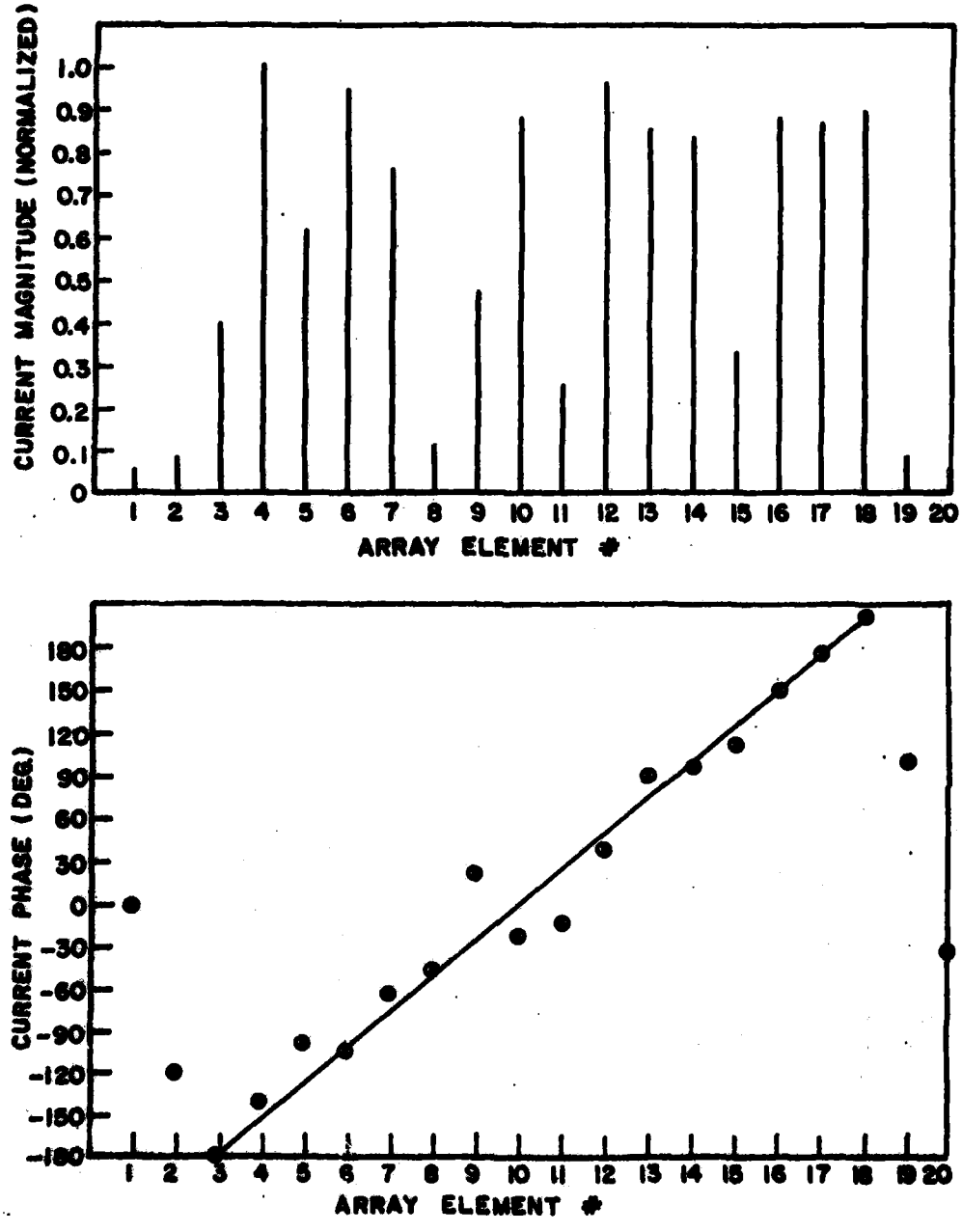

Figure 52: Constrained array current plots (y=15.8 cm).

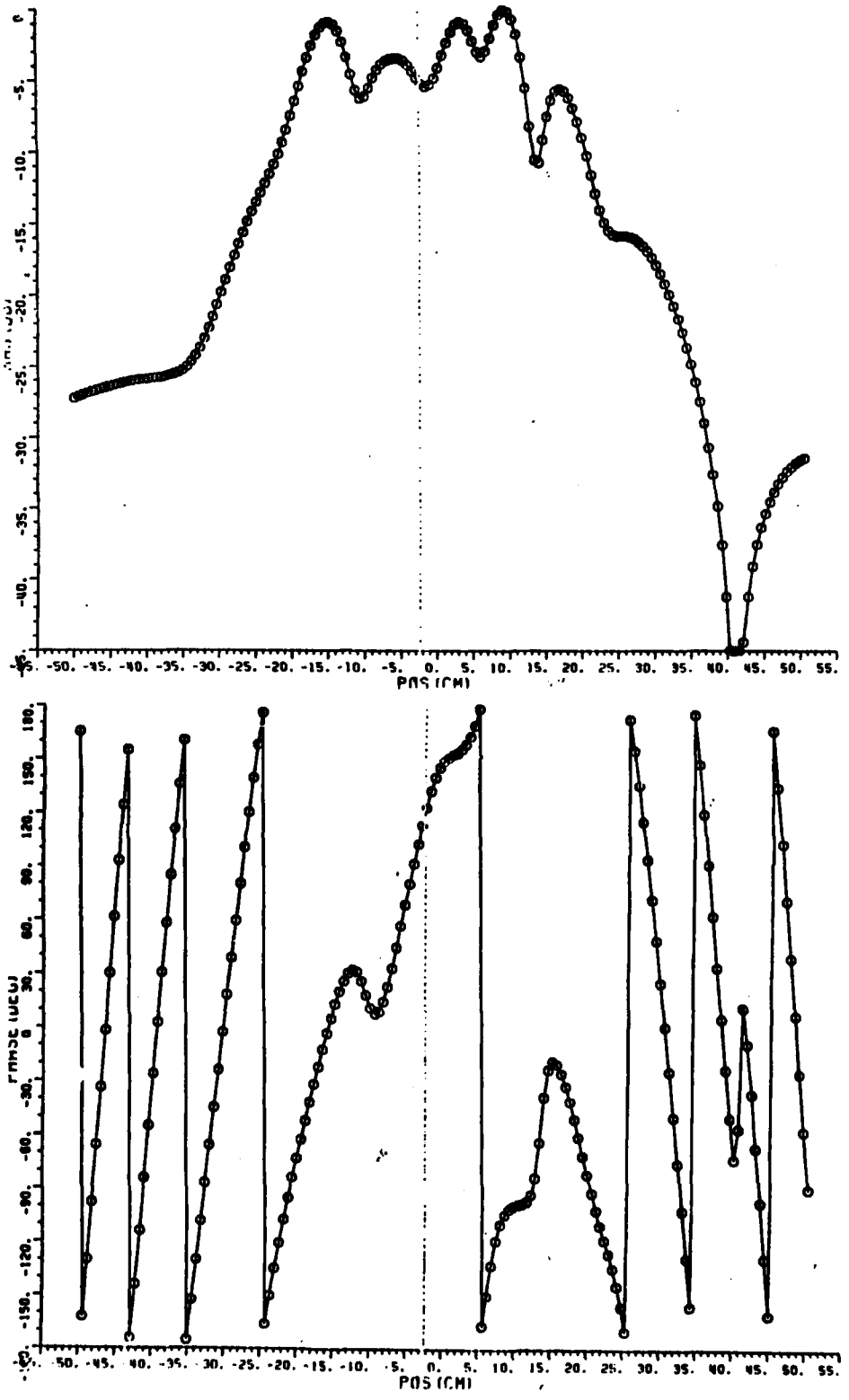

Figure 53: Computed near field for unconstrained currents from y=15.8 cm measurement data (20 elements).

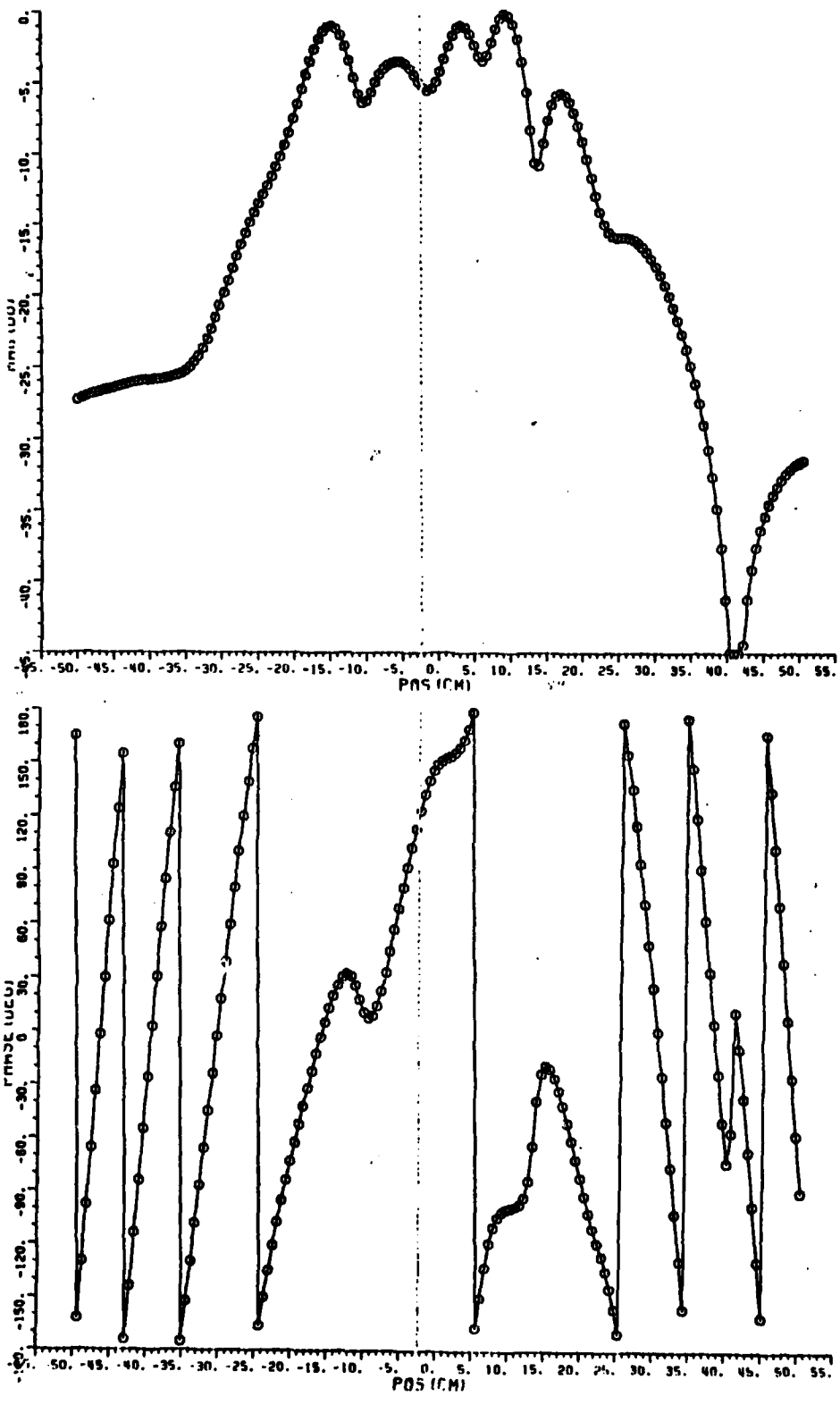

Figure 54: Computed near field for constrained currents from y=15.8 cm measurement data (20 elements).

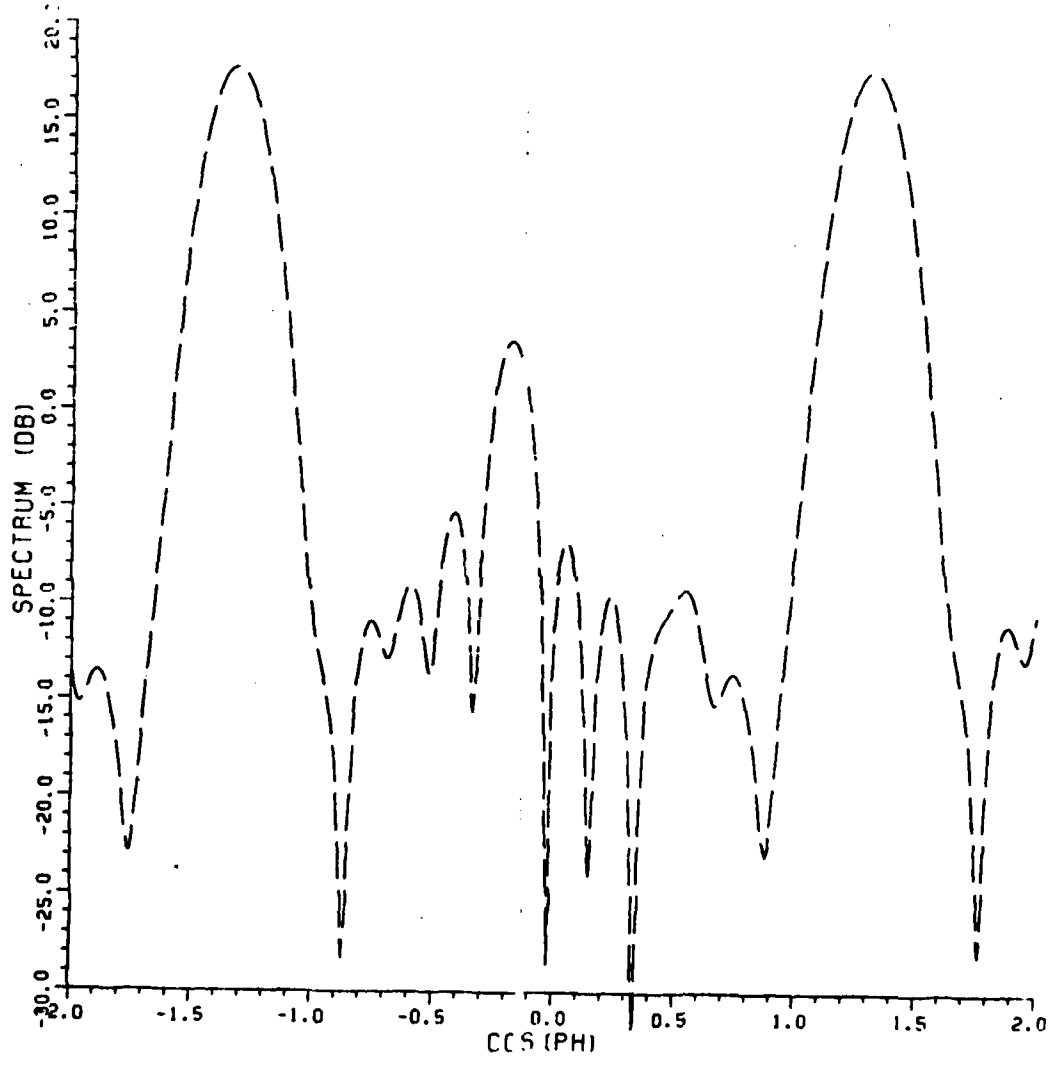

Figure 55: Free space spectrum for unconstrained array currents (y=15.8 cm, 20 elements).

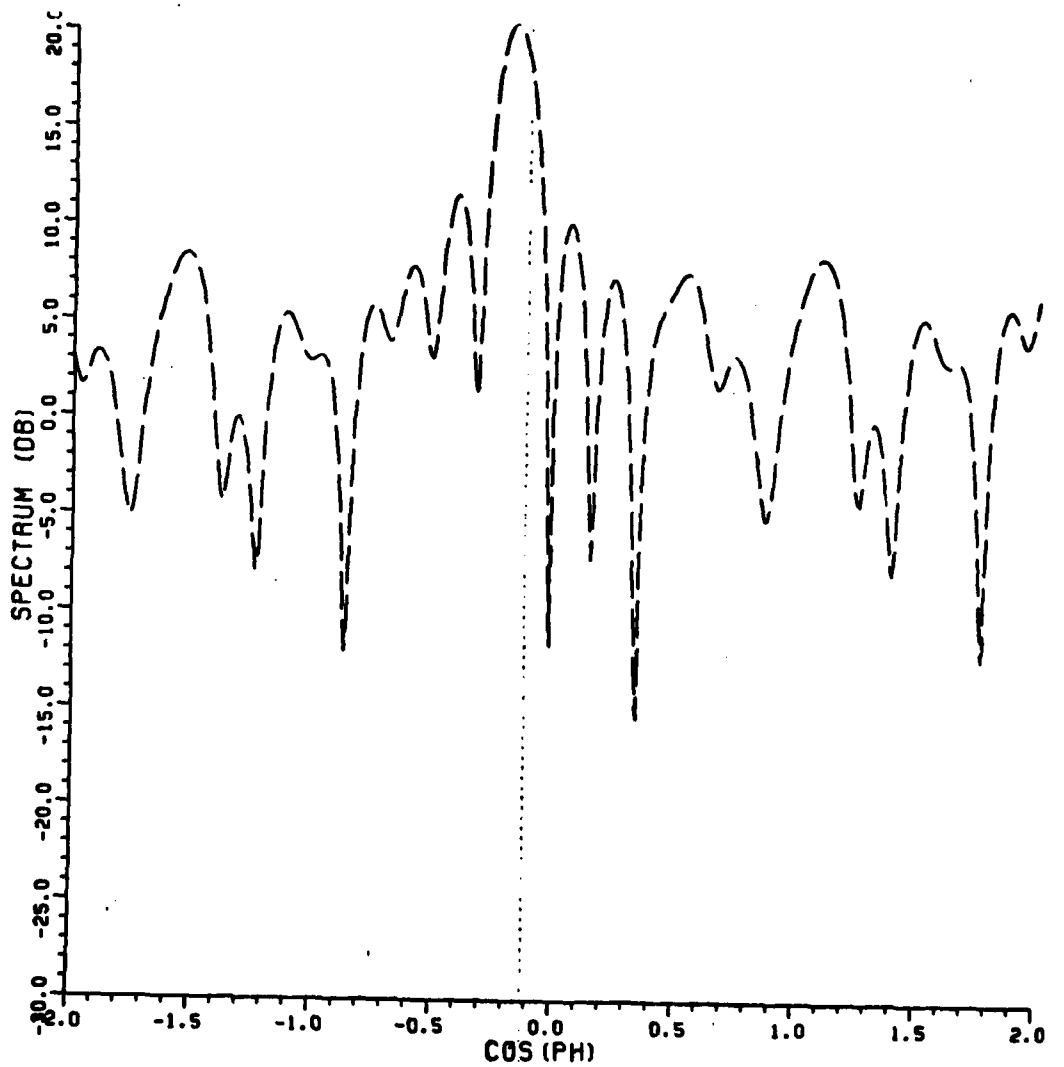

Figure 56: Free space spectrum for constrained array currents (y=15.8 cm, 20 elements).

visible regions with the 16 element case being more reactive. In both cases the constraint was the smallest value, C, in Eq.(9e) which just began to visibly change the Fresnel pattern. The Fresnel region plots are shown in figures 57 and 58 and they correlate well with the measurement of figure 50. Thus it can be seen that including the additional 4 passive elements in the antenna model and solving for the 20 excitations added little to the results except to provide a slightly less reactive current solution with good radiated field correlation.

E. ALGORITHM FOR DETERMINING A GOOD CURRENT SOLUTION

The constrained solutions of the two previous cases seem to be close to the best currents which could be found through the techniques discussed so far. From the cases described in Section V it is clear that more heavily constrained currents would be less accurate than those of figures 42 and 53 since the currents of much greater constraint would not have radiated fields which correlate well with measurements. Also, currents which were much less constrained could not be a better solution since these would exhibit much greater reactivity. These cases, then, suggest that there is at least a range of constrained solutions which have radiation characteristics that closely approximate the measured radiation characteristics of the antenna and have reasonable quality factors.

Experience in applying constraints in trail and error fashion to obtain reasonable solutions also suggest that there is a range of best solutions. It turns out that as the source norm constraint is first being increased through a trial and error process the quality number is decreasing rapidly and the pattern error is increasing slowly. As the constraint is further increased a breakpoint(or rather break-area) is reached afterwhich the quality number reduction slows and the pattern error increases rapidly. The constrained current sets of this section whose radiated patterns just deviate from the radiated patterns of the unconstrained set were near this so called breakpoint and were almost the same as the other current distributions near this breakpoint. Thus any current solution near this breakpoint is among the best solutions which can be found. These solutions will accurately radiate the fields of the array and have reasonable reactivities, which provides the most realistic representation to the actual excitation.

Evidence that different current solutions near the breakpoint are similar is given through tables 11 through 13 and figures 59 through 64. These tables and figures show different current solutions and free space far field spectrums corresponding to the measurement data of figure 41 and a twenty element current solution. The currents of table 11 and figure 59, and the spectrum of figure 62 are the same as those of table 10, figure 52, and figure 56 respectively. These currents were computed

TABLE 11

CONSTRAINED ARRAY CURRENTS FOR y=15.8 cm MEASUREMENTS
ALONG WITH SOURCE NORM, PATTERN ERROR,
AND QUALITY NUMBER

ARRAY ELEMENT #	CURRENT MAGNITUDE	CURRENT PHASE
1	0.0483	-5.281
2	0.0769	-121.4
3	0.392	-180.0
4	1.00	-142.8
5	0.618	-100.5
6	0.949	-107.4
7	0.752	-64.99
8	0.111	-50.32
9	0.479	19.50
10	0.888	-26.96
11	0.252	-17.91
12	0.965	35.46
13	0.856	88.47
14	0.831	95.36
15	0.331	108.8
16	0.888	149.8
17	0.873	174.0
18	0.899	-161.0
19	0.0854	97.03
20	0.0496	-36.31
$\|f'\|=1.45\times10^{-3}$,	$E=8.02\times10^{-4}$,	$Q=1.11\times10^{-5}$

TABLE 12

CONSTRAINED ARRAY CURRENT FOR y=15.8 cm MEASUREMENTS
ALONG WITH SOURCE NORM, PATTERN ERROR,
AND QUALITY NUMBER

ARRAY ELEMENT #	CURRENT MAGNITUDE	CURRENT PHASE
1	0.0458	4.849
2	0.0846	-118.1
3	0.329	-180.0
4	0.941	-137.5
5	0.488	-92.66
6	0.922	-103.8
7	0.612	-55.73
8	0.167	-59.34
9	0.404	34.83
10	0.898	-22.06
11	0.091	-29.35
12	1.00	34.84
13	0.747	105.9
14	0.784	88.35
15	0.318	137.9
16	0.743	148.0
17	0.827	-178.8
18	0.768	-157.4
19	0.0675	110.8
20	0.0440	-26.79
$\|f'\|=1.50\times10^{-3}$,	$E=8.01\times10^{-4}$,	$Q=1.19\times10^{-5}$

TABLE 13

CONSTRAINED ARRAY CURRENT FOR y=15.8 cm MEASUREMENTS
ALONG WITH SOURCE NORM, PATTERN ERROR,
AND QUALITY NUMBER

ARRAY ELEMENT #	CURRENT MAGNITUDE	CURRENT PHASE
1	0.0387	10.03
2	0.0759	-113.1
3	0.280	-180.0
4	0.797	-133.3
5	0.380	-93.90
6	0.806	-97.52
7	0.433	-57.61
8	0.249	-41.38
9	0.279	63.45
10	0.931	-17.90
11	0.125	-173.2
12	1.00	30.42
13	0.696	122.9
14	0.695	78.14
15	0.353	156.2
16	0.570	144.2
17	0.744	-174.8
18	0.618	-155.1
19	0.0551	124.9
20	0.0382	-19.96
$\|f'\|$=1.60x10-3,	E=8.00x10-3,	Q=1.35x10-5

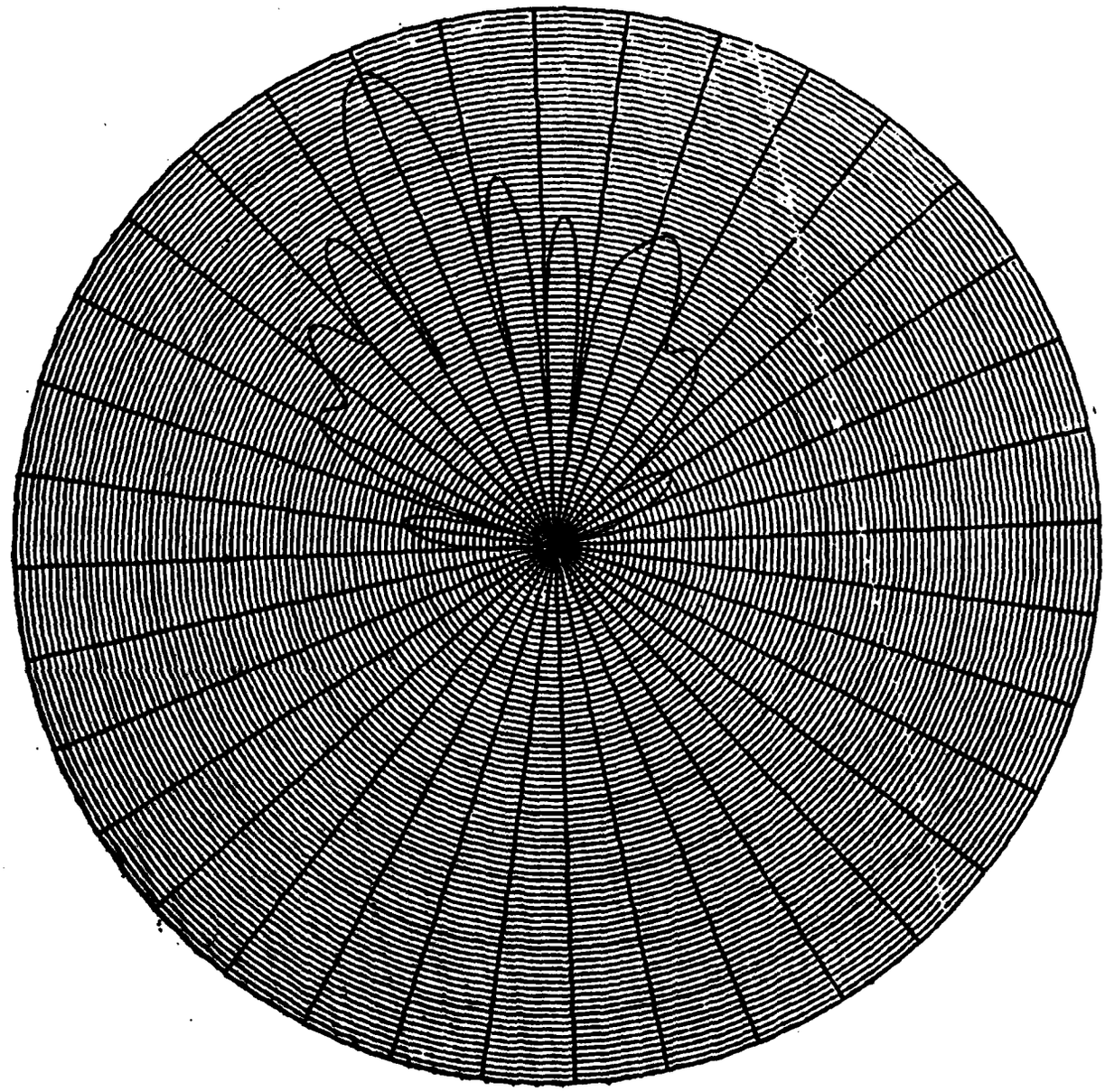

Figure 57: Computed fresnel region pattern of array for the constrained currents corresponding to y=15.8 cm near field measurements (20 elements).

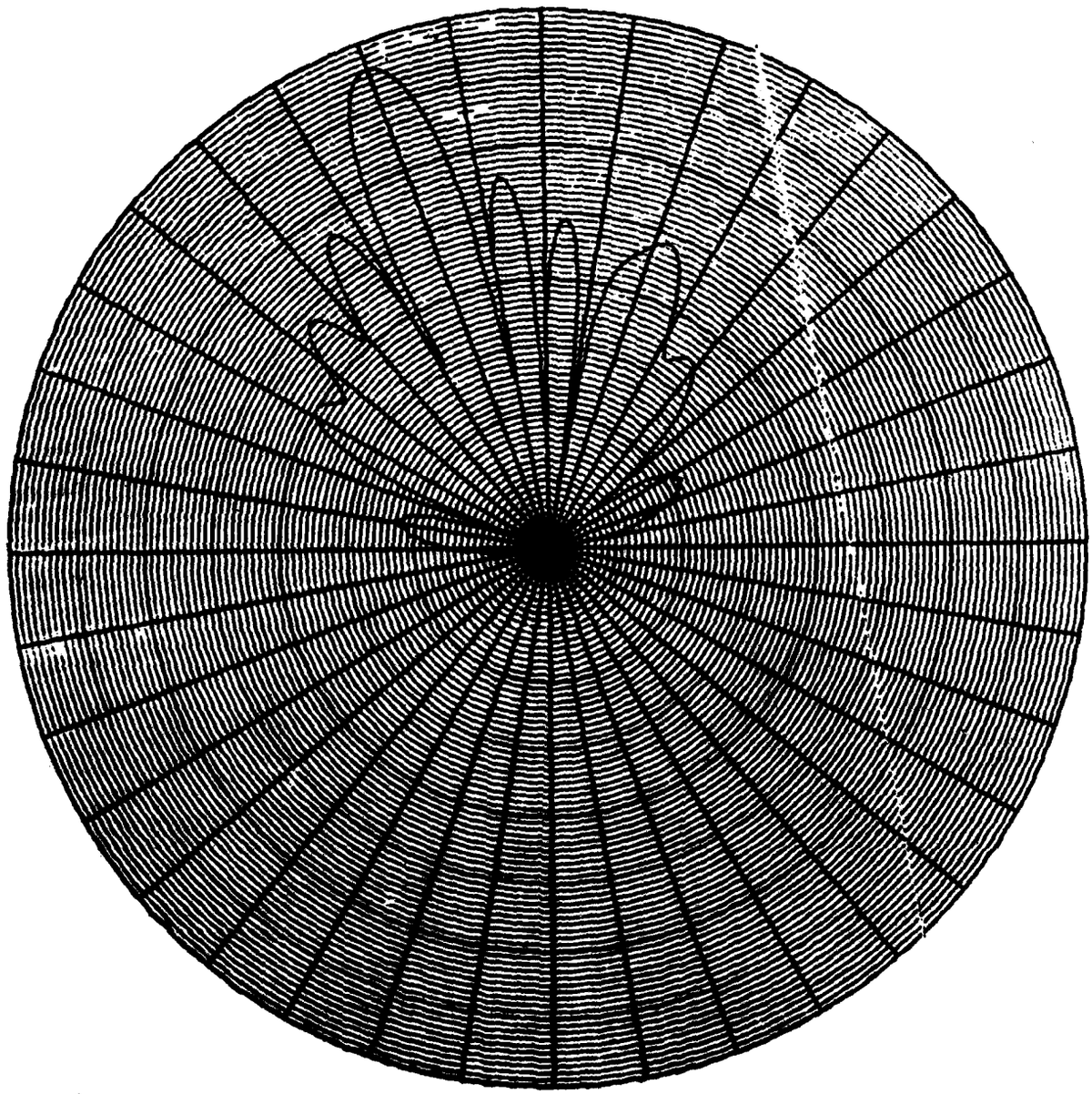

Figure 58: Computed fresnel region pattern of array for the unconstrained currents corresponding to y=15.8 cm near field measurements (20 elements).

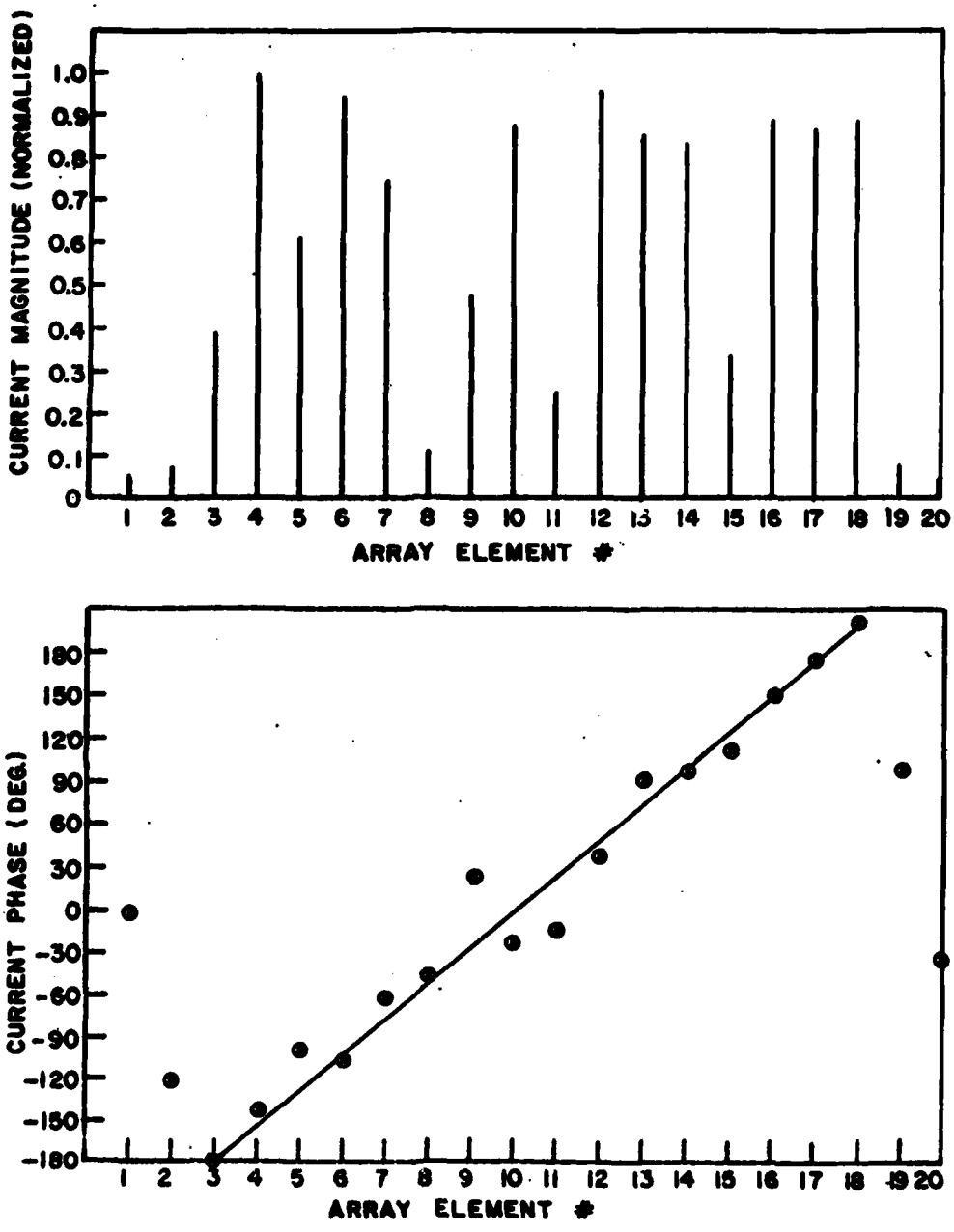

Figure 59: Constrained array current plots (y=15.8 cm, $|\epsilon|=1.45\times10^{-3}$)

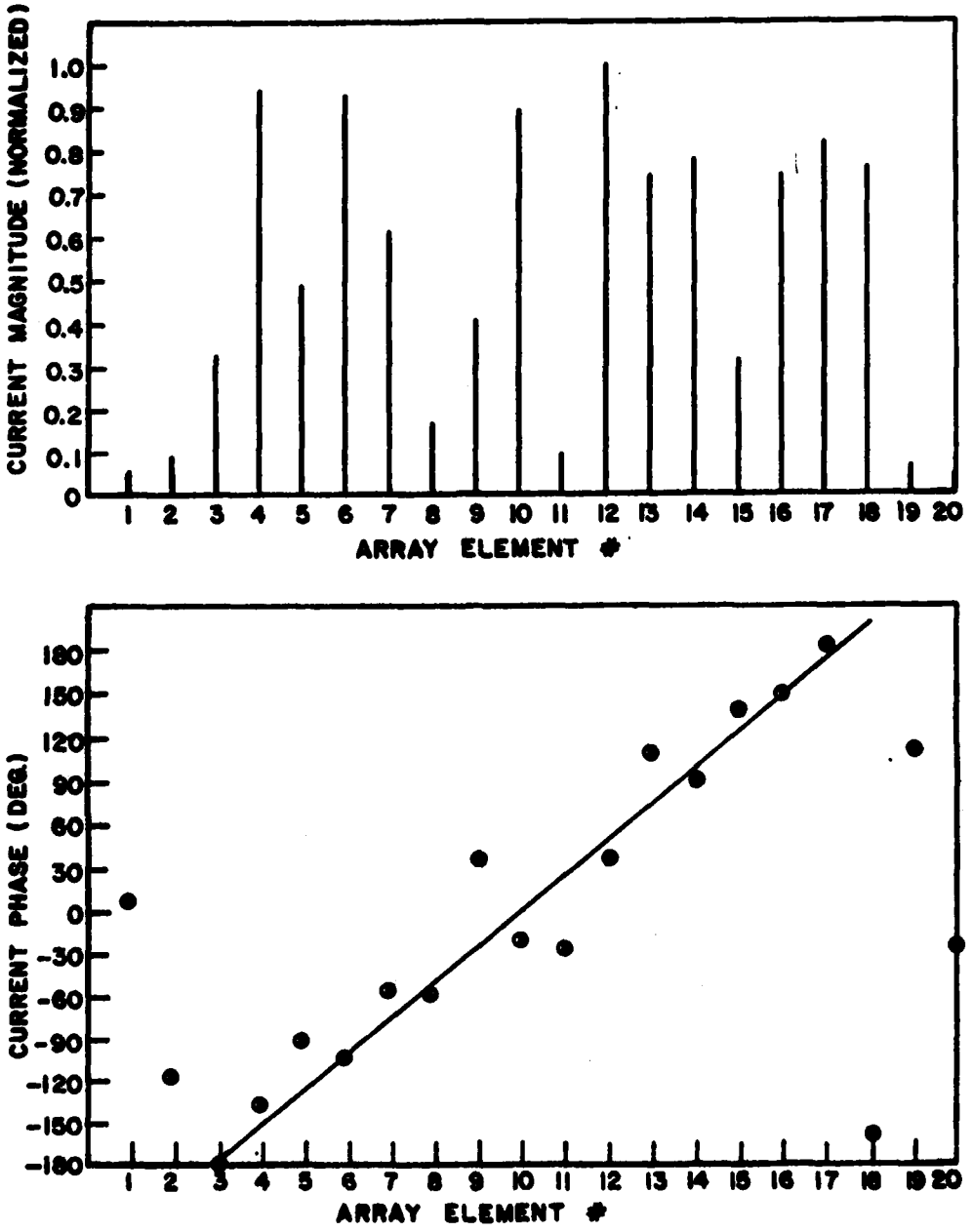

Figure 60: Constrained array current plots (y=15.8 cm, $|\varepsilon|=1.50\times10^{-3}$)

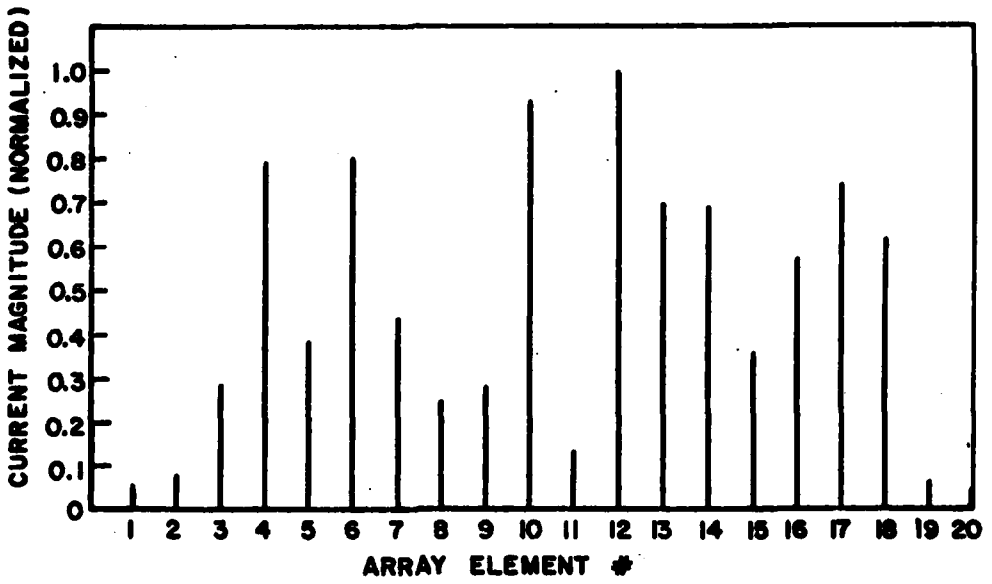

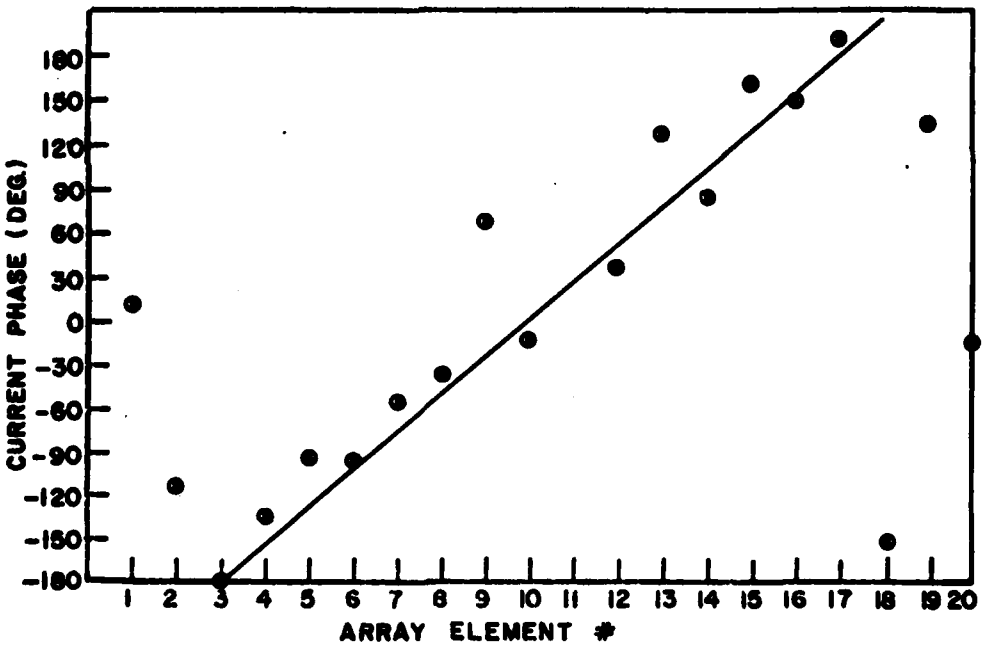

Figure 61: Constrained array current plots (y=15.8 cm, $\|\varepsilon\|=1.6\times10^{-3}$)

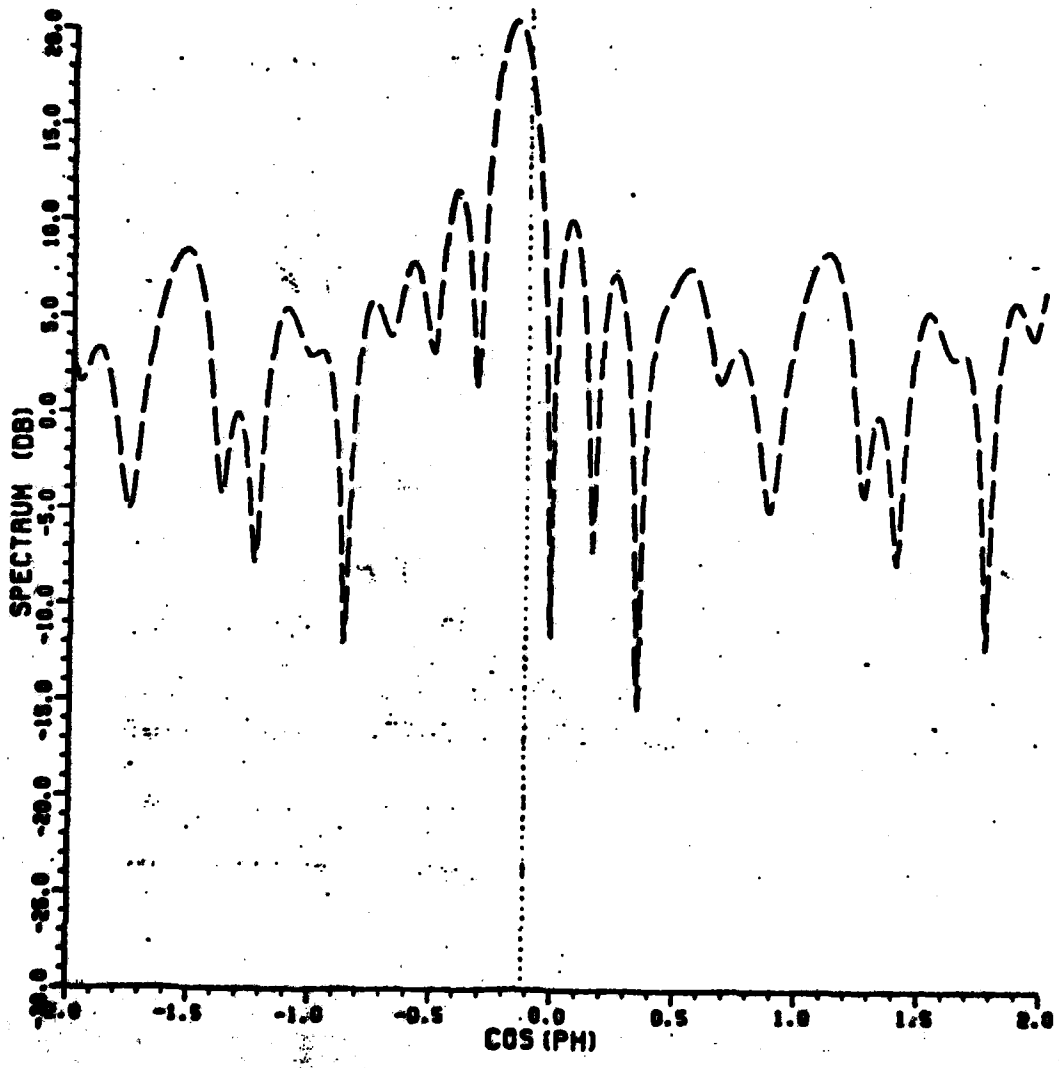

Figure 62: Free space spectrum for constrained array currents ($||f'||=1.45\times10^{-3}$, y=15.8 cm, 20 elements).

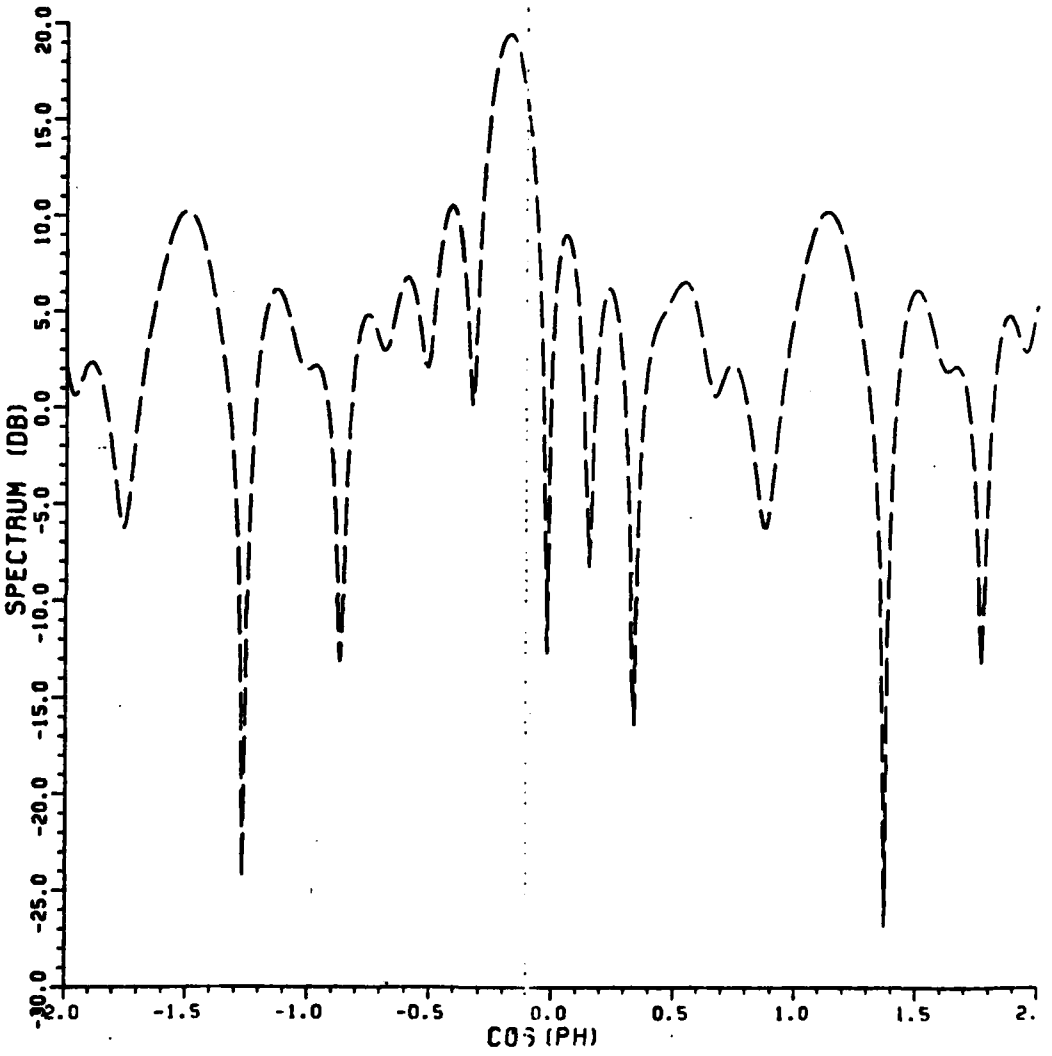

Figure 63: Free space spectrum for constrained array currents ($||f'||=1.5\times10^{-3}$, y=15.8 cm, 20 elements).

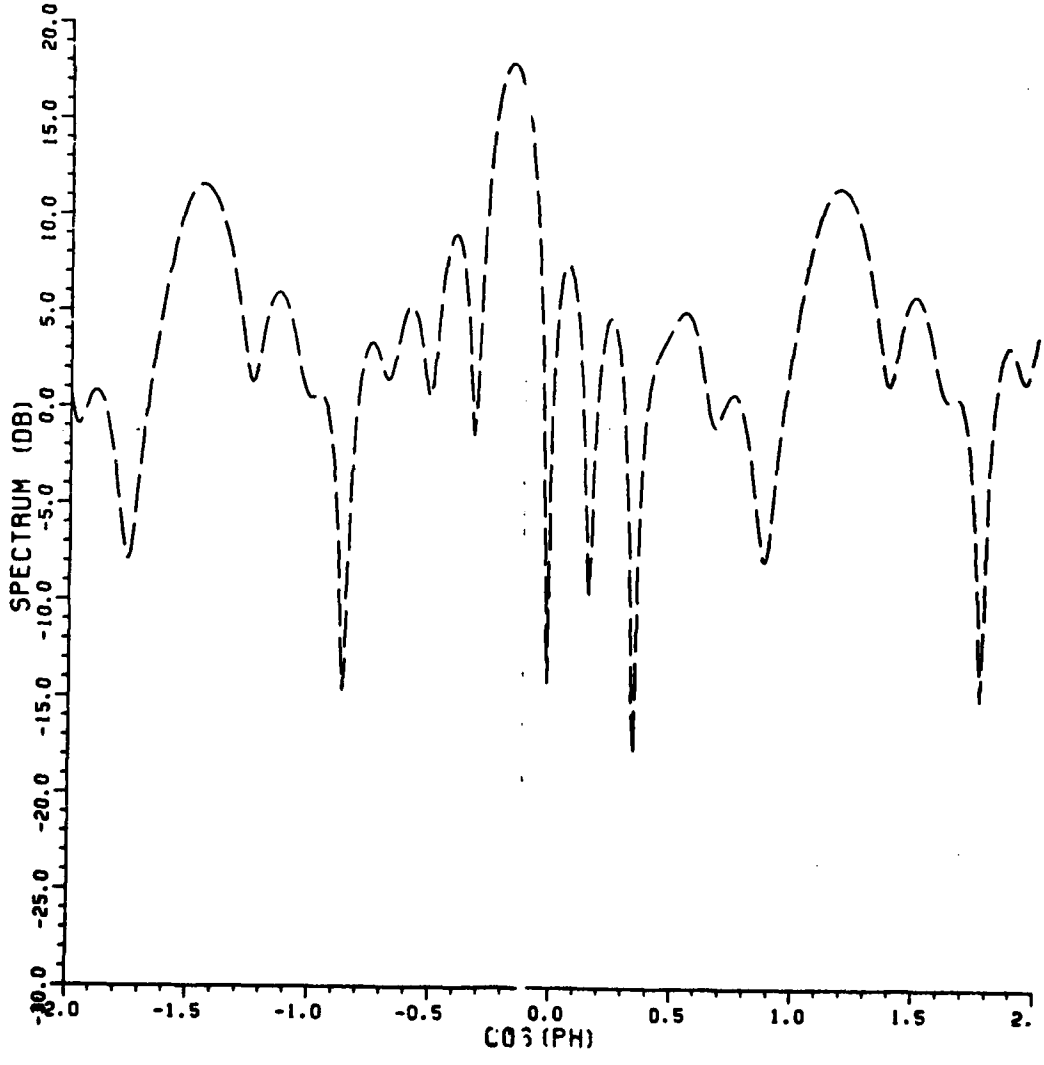

Figure 64: Free space spectrum for constrained array currents ($||f'||=1.60\times10^{-3}$, y=15.8 cm, 20 elements).

with different source norm constraints. The constraints of the currents of figures 60 and 61 were less than the constraint corresponding to the solution of figure 59. Since the fields of the currents of figure 59 just began to noticeably deviate from the measurements, tighter constraints are less accurate from a radiation point of view. It is clear that the distributions of figures 59 and 60 are quite similar. Also, the spectrums reveal reasonable near field stored energy. Based on the apriori knowledge of the antenna, then, either solution is admissible. Although the solution of figure 61 has somewhat different individual magnitudes and phases than the other two solutions the overall magnitude and phase distributions follow the same trends as the other two. However, the spectrum of figure 64 indicates it is just begining to show excessive amounts of near field stored energy. This solution is, then, a borderline case and its admission as a reasonable set of currents is a matter of judgement.

An algorithm, then, which may result in a good approximation to the currents which exist on an array which is assumed not to be highly reactive is as follows:

1) Using the near field measurements and Eqs.(9) compute an unconstrained solution.

2) Use the unconstrained currents to compute and plot various radiation distributions which are of interest(near field, Fresnel field, or far field). The radiated fields of these currents are a best approximation to the actual radiated fields of the array.

3) Using the computed radiated fields as a guide reduce the constraint in a trial and error process by various factors and compute constrained currents. For each set of constrained currents compute and plot radiated fields which correspond to the fields of step 2.

4) Find a set of constrained currents which correspond to a radiated field plot which just begins to noticeably deviate from the radiated field plot of the unconstrained currents. This set of currents will be the least reactive currents which reproduce the radiated field of the antenna.

SECTION VIII

SOURCE DETERMINATION USING ONLY MEASURED MAGNITUDE VALUES

A. INTRODUCTION

The phase iteration algorithm described in Section II was applied to the y=15.8cm near field measurement data of figure 41 with little success. While the algorithm converged to a source solution with small pattern error, the solution was wrong. The currents failed to radiate fields which correlated with measurements. The resultant currents did have a near field magnitude pattern which correlated well with the measured near field pattern yet the pattern phase was appreciably different than that of the measurements. Consequently, the computed Fresnel magnitude and phase patterns did not correlate well with measurements. The computed near field pattern phase corresponding to a source solution did depend upon the initial measurement phase assumption in the solution process.

B. PROCEDURE

Equations 9 and 10 together with the phase iteration algorithm described in Section II were applied to the near field measurement magnitude data of figure 41. In applying this algorithm, three different measurement phase distributions were assumed. These were zero phase for all field values, alternating phase in which every other field point had a 180^0 phase value and all others had a 0^0 phase value, and a piecewise linear phase fit to the measured phase in which two straight lines were drawn between the outermost phase data points and the peak phase value on the plot of figure 41 and all measurement phases were assumed to fall on these lines. Once the near field phase distribution was specified, the currents were computed through Eqs.(9) of Section II according to the algorithm mentioned above. Since the results were so poor only unconstrained current cases are shown. Currents computed with imposed source norm constraint were less reactive and did not have radiated fields which correlated any better with measurements than the fields of constrained currents. In each case mentioned above the iteration procedure was terminated when the pattern error of a particular iteration differed from the pattern error of the last iteration by less than 1 part in 1000.

C. RESULTS

The resulting currents for the three cases mentioned above are shown in tabular form in tables 14 through 16. The computed near fields associated with these currents are shown in figures 65 through 67. The magnitude plots of these computed near fields compare favorably with the plot of figure 41. However, the phase distributions of each case are different than the phase plot of figure 41. Since, according to the equivalence principle, the fields defined over a closed surface uniquely determine all the fields which exist, it is no suprise that the computed Fresnel region plots of figures 68 through 70 are markedly different than the measurement plot shown in figure 50. The comparison of these computed Fresnel plots with the measurements then indicates that the currents computed without any phase knowledge cannot be the actual currents which existed on the array.

TABLE 14

UNCONSTRAINED CURRENTS COMPUTED FROM y=15.8 cm NEAR FIELD MAGNITUDE MEASUREMENT DATA. ZERO INITIAL PHASE DISTRIBUTION ASSUMED

ARRAY ELEMENT #	CURRENT MAGNITUDE	CURRENT PHASE
3	0.085	-180.0°
4	0.153	0.1859°
5	0.341	-176.5°
6	0.488	3.291°
7	0.699	-175.2°
8	0.843	4.365°
9	0.984	-175.0°
10	1.00	6.286°
11	0.996	171.9°
12	0.844	9.154°
13	0.711	-169.0°
14	0.491	13.75°
15	0.352	-162.6°
16	0.171	18.04°
17	0.101	-157.7°
18	0.021	39.86°

TABLE 15

UNCONSTRAINED CURRENTS COMPUTED FROM y=15.8 cm
NEAR FIELD MAGNITUDE MEASUREMENT DATA. 0°/180°
ALTERNATING INITIAL PHASE DISTRIBUTION ASSUMED

ARRAY ELEMENT #	CURRENT MAGNITUDE	CURRENT PHASE
3	0.042	-180.0°
4	0.127	-12.03°
5	0.272	169.0°
6	0.410	-6.294°
7	0.585	-177.4°
8	0.776	-1.397°
9	0.963	-176.9°
10	0.952	11.58°
11	1.00	-167.4°
12	0.962	13.01°
13	0.765	-161.3°
14	0.570	22.05°
15	0.438	-155.2°
16	0.263	25.27°
17	0.113	-153.6°
18	0.067	5.452°

TABLE 16

UNCONSTRAINED CURRENTS COMPUTED FROM y=15.8 cm NEAR FIELD MAGNITUDE MEASUREMENT DATA. PIECEWISE LINEAR INITIAL PHASE DISTRIBUTION ASSUMED

ARRAY ELEMENT #	CURRENT MAGNITUDE	CURRENT PHASE
3	0.045	-180.0°
4	0.068	-31.71°
5	0.195	-171.5°
6	0.349	-24.67°
7	0.490	155.1°
8	0.699	-23.20°
9	0.900	150.4°
10	0.962	-28.93°
11	1.00	153.2°
12	0.934	-31.93°
13	0.757	146.9°
14	0.603	-28.74°
15	0.420	145.3°
16	0.175	-31.63°
17	0.158	156.65°
18	0.063	-80.85°

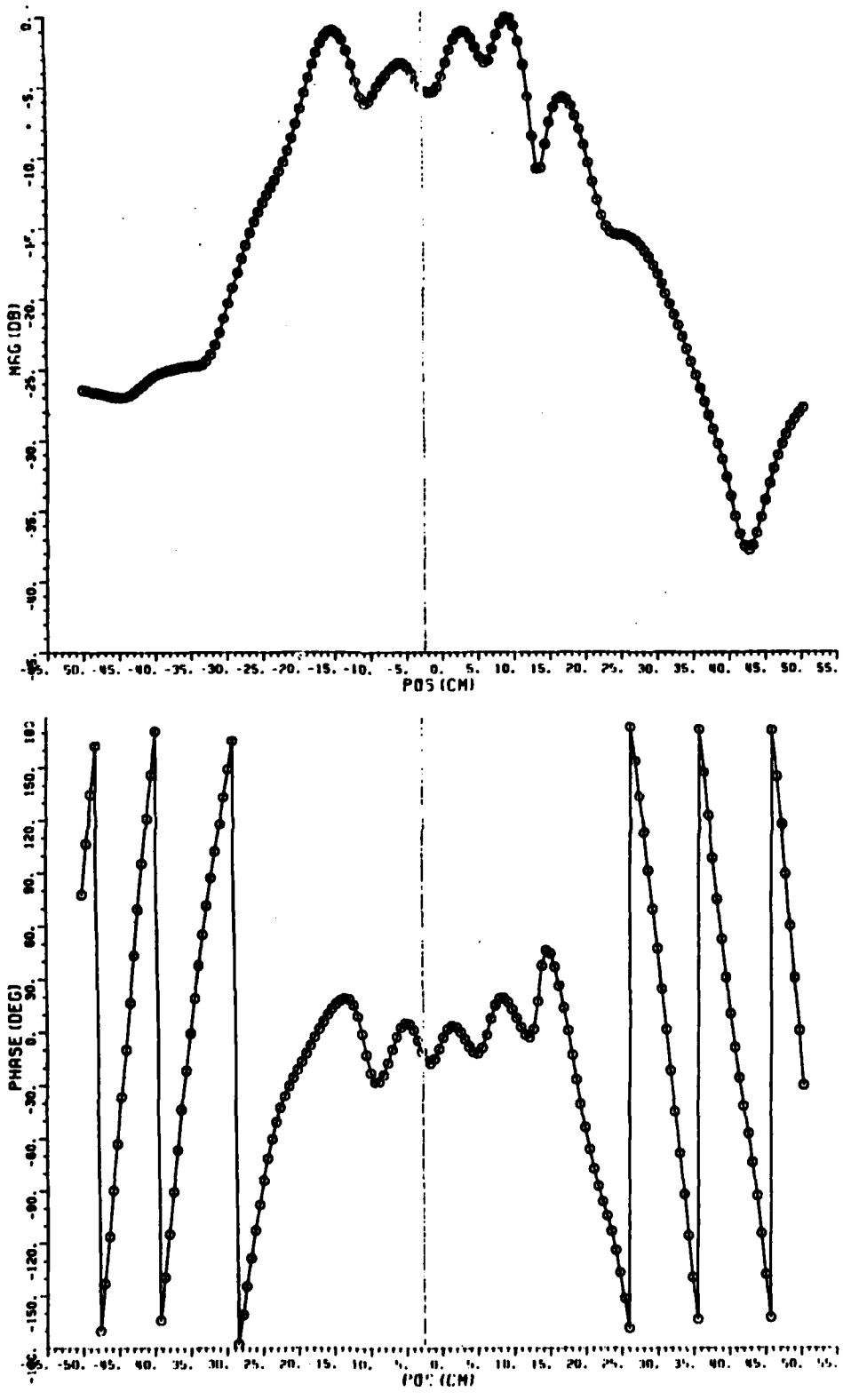

Figure 65: Computed near field for unconstrained currents from y=15.8 cm magnitude measurement data and 0^{o} initial phase assumption.

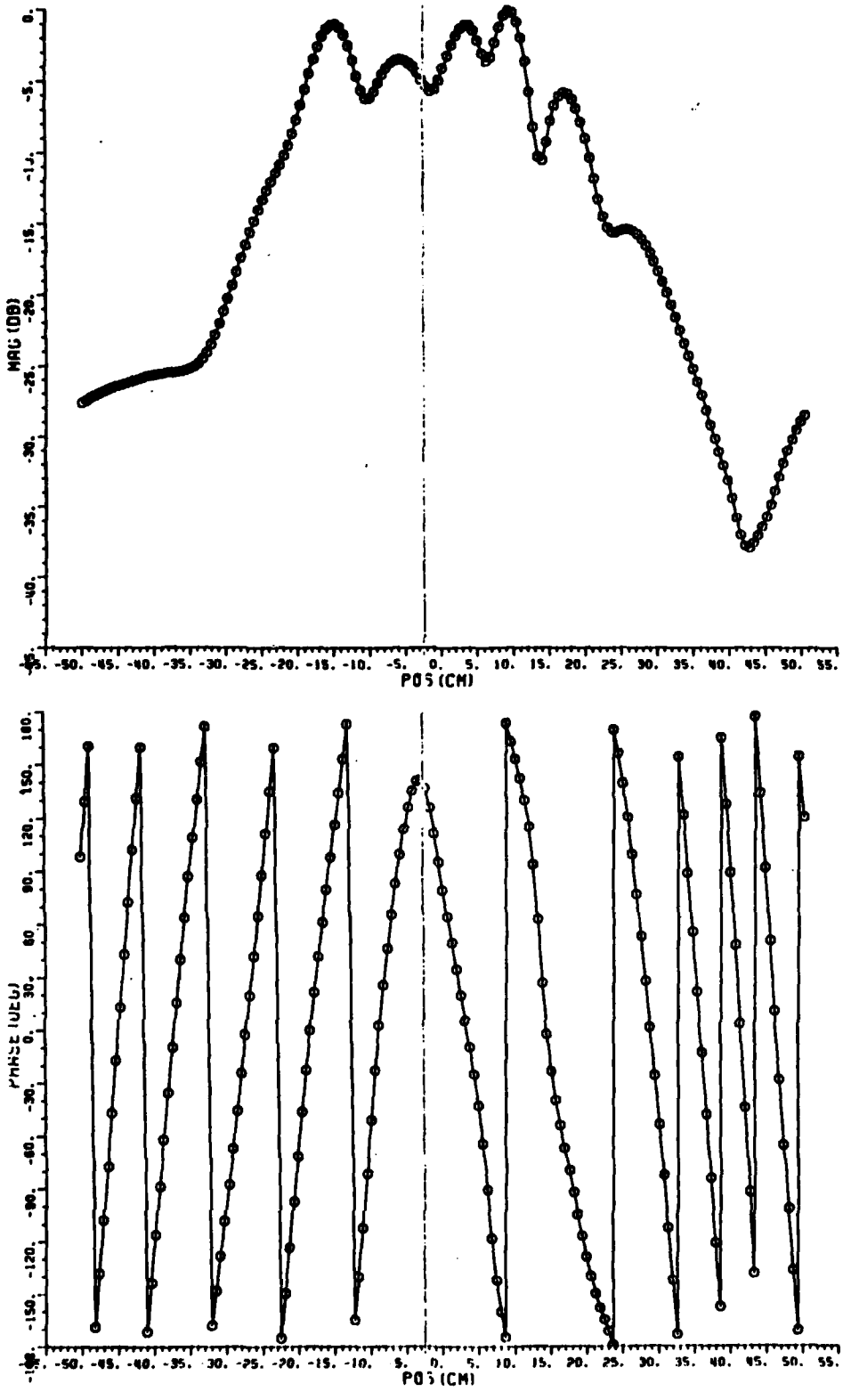

Figure 66: Computed near field for unconstrained currents from y=15.8 cm magnitude measurement data and 0°/180° alternating initial phase assumption.

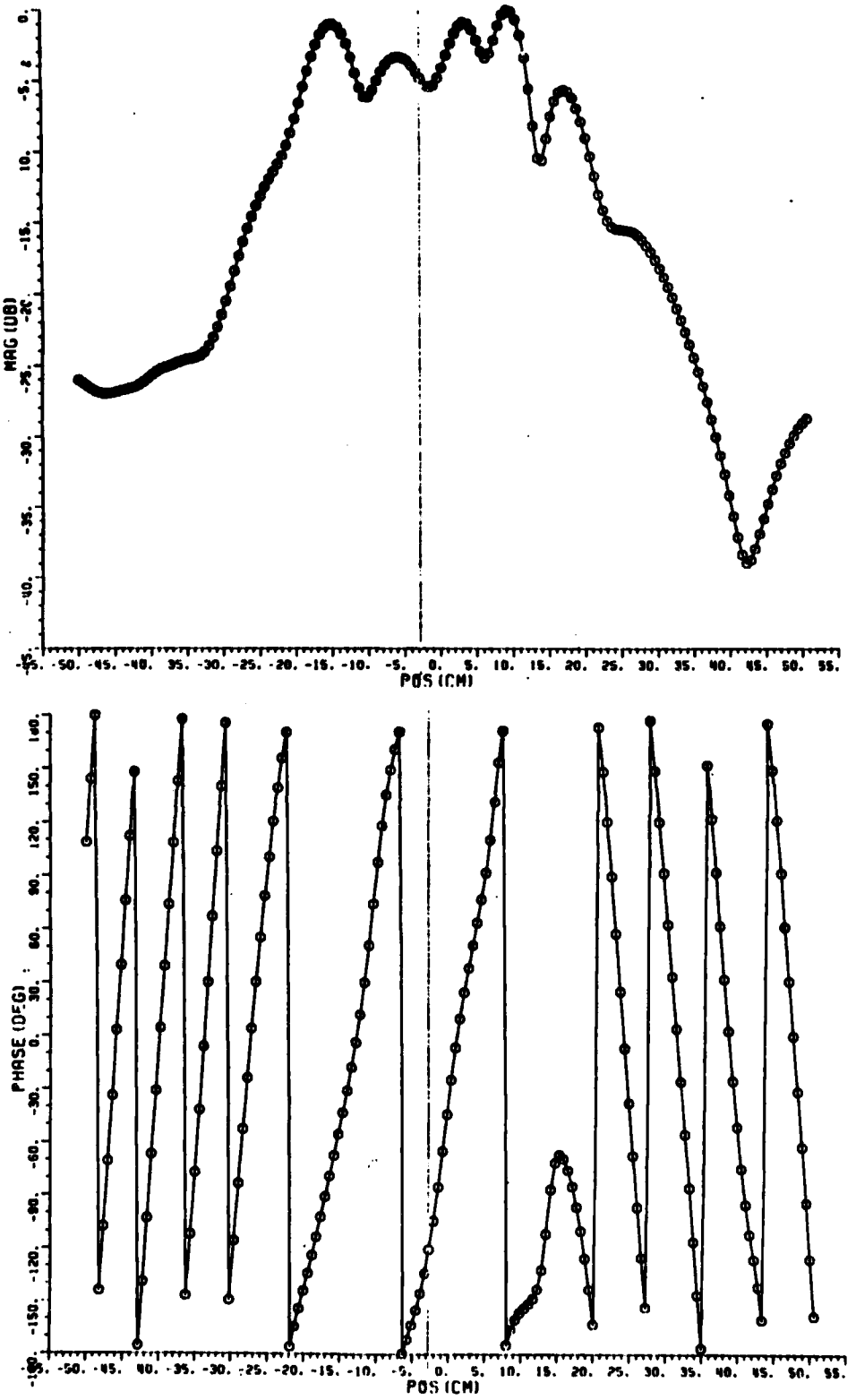

Figure 67: Computed near field for unconstrained currents from y=15.8 cm magnitude measurement data and piecewise linear initial phase assumption.

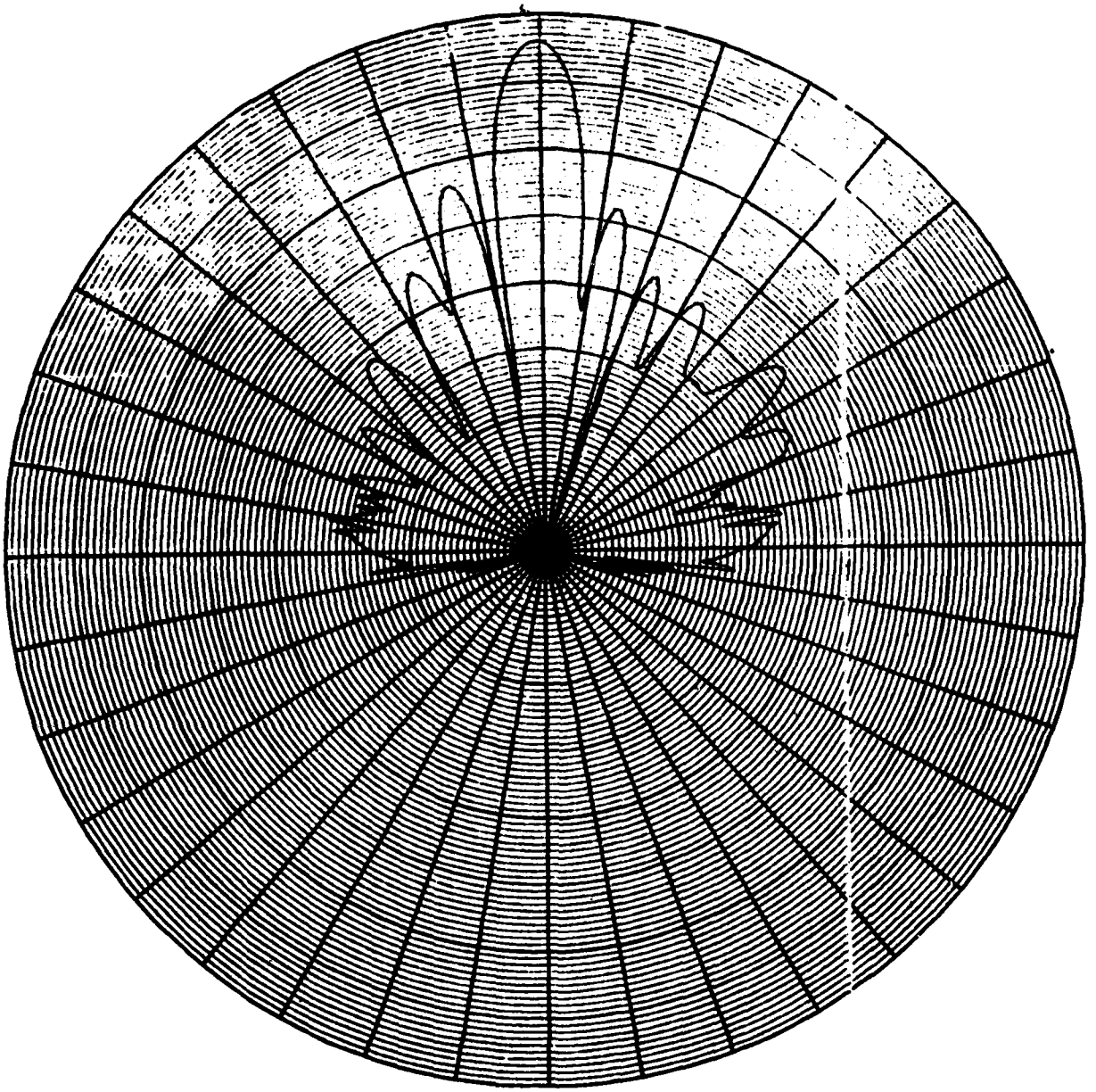

Figure 68: Computed fresnel region pattern of array using unconstrained currents from y=15.8 cm near field magnitude data with 0° initial phase assumption.

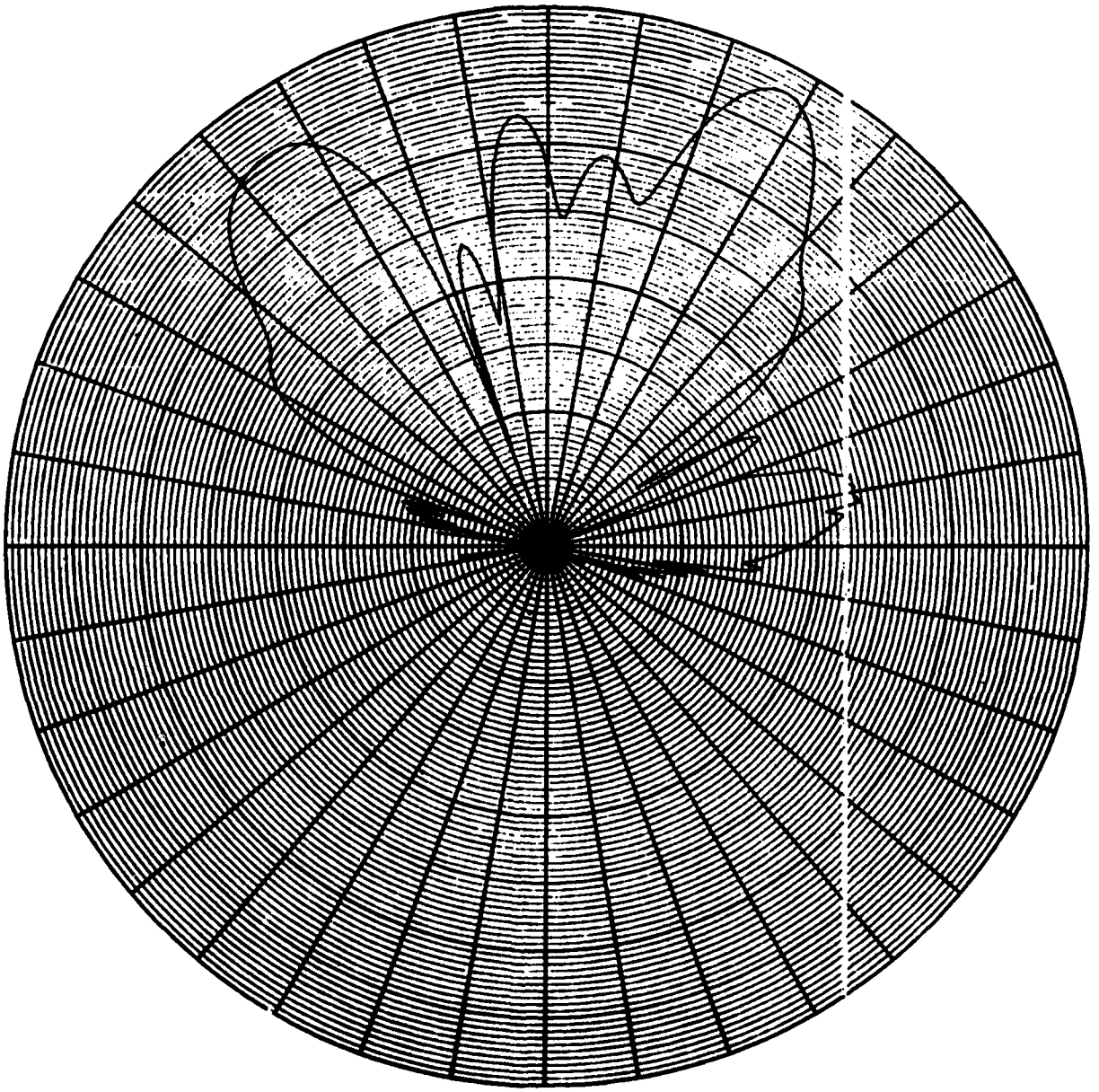

Figure 69: Computed fresnel region pattern of array using unconstrained currents from y=15.8 cm near field magnitude data with 0°/180° alternating initial phase assumption.

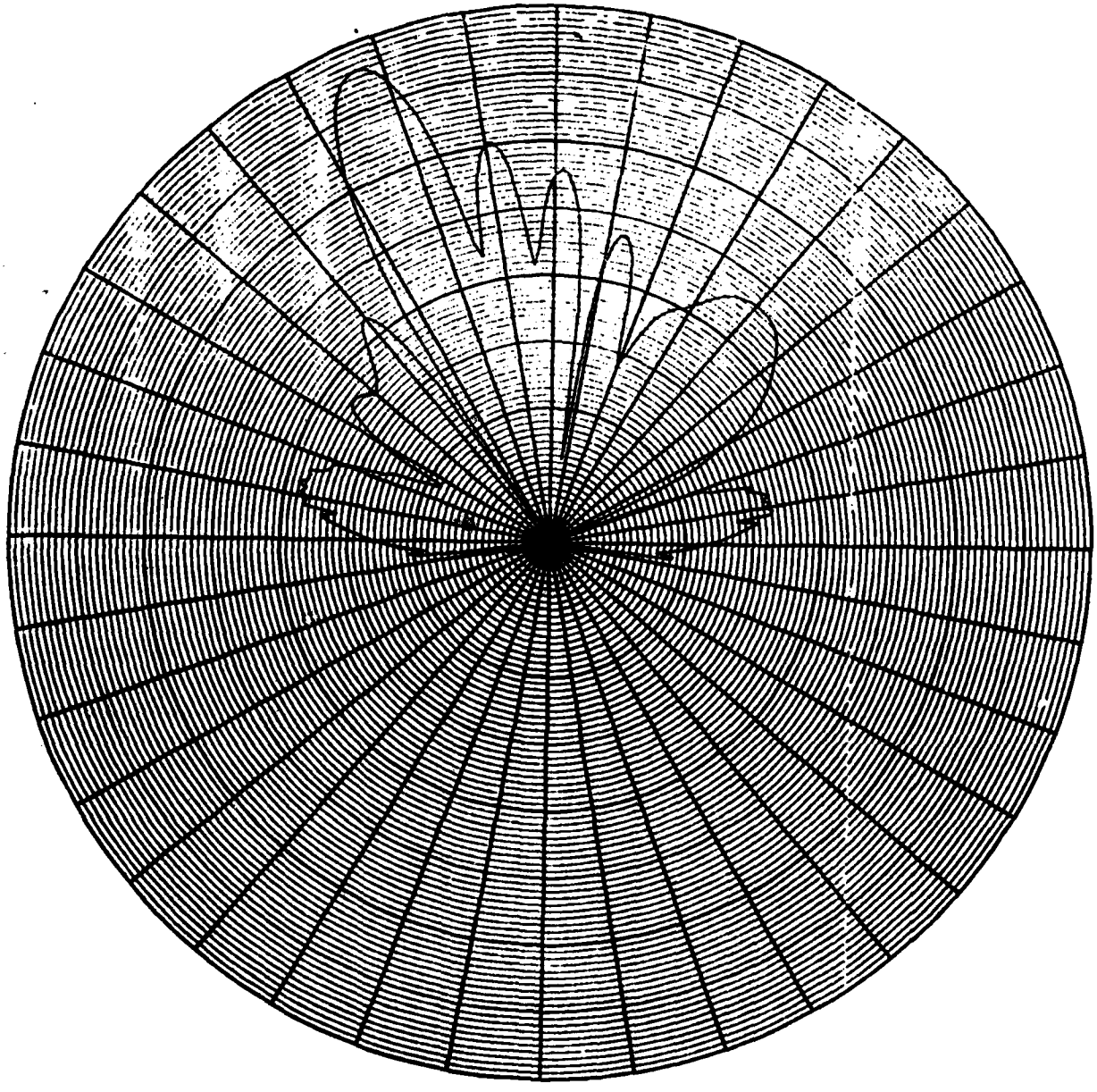

Figure 70: Computed fresnel region pattern of array using unconstrained currents from y=15.8 cm near field magnitude data with piecewise linear initial phase assumption.

SECTION IX

SOLUTION SENSITIVITY TO NEAR FIELD DATA VARIATION

A. INTRODUCTION

Below is an investigation into the sensitivity of the current solution to increased near field sampling distance and decreased range in the measurement process. In demonstrating the effects of measurement data variation on the solution the near field data of figure 41 will be used. Also, currents of constrained norm will not be considered since unconstrained currents will be sufficient to indicate trends.

The sensitivity of the antenna currents to increased sampling distance will be accomplished by choosing equally spaced data points from the plot of figure 41. The currents of Section VII, for example, were computed using points spaced slightly less than 0.1λ apart. This included every data point of figure 41. In computing currents using measurements taken every 0.2λ apart every other data point of figure 41 can be used. The number of data points in this case will be half of the number used for the 0.1λ case but the number is still large enough so that insufficient data this is not a significant factor. The measurement spacings considered are, when referenced to figure 4, $\Delta\chi=0.1\lambda$, 0.2λ, 0.4λ, and 0.8λ. The first example corresponds to the case presented in Section VII.

The effects of decreased measurement range can also be shown using the data of figure 41. In this case the data points used are all points within a specified range on the line of measurement centered on the point (x=0,y=15.8cm,z=0) of figure 4. The cases considered are, when referenced to figure 4, $-50\text{cm} < x < 50\text{cm}$, $-37\text{cm} < x < 37\text{cm}$, $-25\text{cm} < x < 25\text{cm}$, and $-18\text{cm} < x < 18\text{cm}$. The first example corresponds to the case presented in Section VII.

The currents are computed through the technique described in Section V. Also, the accuracy assements are made through the same techniques used in Section VI.

B. INCREASED SAMPLING DISTANCE

Table 17a provides a summary of the sampling distance cases mentioned above. The resultant currents corresponding to these cases

TABLE 17a

SUMMARY OF VARIOUS SAMPLING DISTANCE CASES STUDIED

CASE #	SAMPLING DISTANCE (ΔX)	# POINTS USED
Case I	$\Delta X = 0.598$ cm $\approx 0.01\lambda$	169 pts
Case II	$\Delta X = 1.20$ cm $\approx 0.2\lambda$	85 pts
Case III	$\Delta X = 2.39$ cm $\approx 0.4\lambda$	43 pts
Case IV	$\Delta X = 4.79$ cm $\approx 0.8\lambda$	22 pts

are shown in table 17b. These currents change gradually with increased distance and the case, $\Delta x=0.4\lambda$, is not much different from the $\Delta x=0.1\lambda$ case. The case, $\Delta x=0.8\lambda$, seems to deviate significantly from the original case. This may be due to the fact that only 22 data points were used in computing 16 current excitations.

Computed near field magnitude plots for the four cases are shown in figures 72 and 73. The plots correlate well with noticeable discrepancies occuring only in the $\Delta x=0.8\lambda$ case. Fresnel region plots are shown in figure 74 and all but the $\Delta x=0.8\lambda$ case compare well with the measured result. The $\Delta x=0.8\lambda$ case deviates in the sidelobes.

The currents and field plots of table 17b and figures 72 through 74 suggest that the sampling distance can be increased to a value between $\Delta x=0.4\lambda$ and $\Delta x=0.8\lambda$ without decreased accuracy. More importantly, the number of measurement data points required could have been less than 43 which is a reduction from the 169 points used in previous sections by a factor of almost 3.

C. DECREASED MEASUREMENT RANGE

Table 18a provides a summary of the cases of restricted measurement range mentioned above. The computed currents corresponding to those cases are shown in table 18b. Unlike the currents of varied sampling, the currents of table 18b show great change with decreased range. A comparison of the free space far field spectrums corresponding to these currents can be made through figure 76. The trend indicated by these plots seems to be increasing lobes in the invisible region with slight measurement range restriction. Greater restriction results in modification of the exterior portion of the visible region. Finally, further restriction of the range of measurement affects the entire far field pattern. The computed near field magnitude plots of figure 77 show increased discrepancies in the outer portions of the patterns with increased measurement range restriction. The phase plots of figure 78 show little deviation except in the $-18\text{cm} < x < 18\text{cm}$ case in which there is significant change. The Fresnel plots of figure 79 show serious problems only in the $-25 < x < 25$ and $-18 < x < 18$ cases.

The currents and plots of table 18b and figures 76 through 79 demonstrate extreme sensitivity of the solution to a change in measurement range. The free space far field plots are especially informative since they suggest that the reason for the unconstrained current inconsistencies among solutions corresponding to different near field pattern cuts found in Section V is related to the portion of significant radiated energy which the measurements represent. Also, it is obvious from the near field and Fresnel region plots that accurate reproduction of the radiated fields of an array by the computed currents

TABLE 17b

RESULTANT CURRENTS FOR VARIOUS NEAR FIELD
SAMPLE INCREMENTS

	ΔX=0.1λ		ΔX=0.2λ		ΔX=0.4λ		ΔX=0.8λ	
Elem #	Mag	ph	Mag	ph	Mag	ph	Mag	ph
3	0.126	-180.0	0.144	-180.0	0.150	-180.0	0.029	-180.0
4	0.205	160.3	0.219	170.6	0.204	174.8	0.157	-162.5
5	0.418	-128.0	0.433	-127.3	0.429	-128.9	0.124	-113.2
6	0.123	56.69	0.081	35.38	0.080	25.80	0.076	134.4
7	0.696	-123.6	0.692	-121.8	0.693	-120.3	0.386	-92.00
8	0.643	37.90	0.622	36.67	0.623	41.92	0.430	78.02
9	0.670	-135.9	0.619	-135.8	0.642	-127.3	0.617	-99.09
10	0.860	15.85	0.859	13.87	0.839	23.19	0.750	65.78
11	0.786	-146.3	0.739	-145.2	0.768	-134.0	0.899	-106.5
12	1.00	21.16	1.00	22.74	1.00	31.97	1.00	64.11
13	0.475	-175.1	0.439	-178.8	0.398	-160.9	0.745	-113.0
14	0.680	35.52	0.670	40.75	0.693	49.55	0.813	66.91
15	0.333	-173.1	0.313	-172.4	0.294	-158.9	0.493	-117.2
16	0.311	74.26	0.325	84.83	0.357	89.27	0.430	78.91
17	0.335	168.6	0.357	171.5	0.343	174.3	0.274	-148.9
18	0.199	158.7	0.223	164.0	0.233	165.2	0.069	133.5

TABLE 18a

SUMMARY OF MEASUREMENT RANGE
RESTRICTION CASES STUDIED

CASE #	MEASUREMENT RANGE	# POINTS USED
Case I	-50 cm <X< 51 cm	169 pts
Case II	-37 cm <X< 37 cm	124 pts
Case III	-25 cm <X< 25 cm	84 pts
Case IV	-18 cm <X< 18 cm	60 pts

TABLE 18b

RESULTANT CURRENTS FOR VARIOUS NEAR FIELD SAMPLE INCREMENTS

	-50cm<X<51cm		-37cm<X<37cm		-25cm<X<25cm		-18cm<X<18cm	
Elem #	Mag	ph	Mag	ph	Mag	ph	Mag	ph
3	0.126	-180.0	0.088	-180.0	0.026	-180.0	0.017	-180.0
4	0.205	160.3	0.125	123.6	0.079	40.73	0.342	-74.5
5	0.418	-128.0	0.393	-142.6	0.236	-172.4	0.735	46.61
6	0.123	56.69	0.292	27.03	0.350	-0.475	0.876	-166.0
7	0.696	-123.6	0.728	-148.0	0.600	175.1	1.00	-11.05
8	0.643	37.90	0.795	16.52	0.771	-10.78	0.708	134.9
9	0.670	-135.9	0.837	-164.1	0.910	168.8	0.345	-101.3
10	0.860	15.85	1.00	0.1647	1.00	-12.94	0.439	22.76
11	0.786	-146.3	0.880	-172.4	0.987	-187.5	0.600	166.67
12	1.00	21.16	0.964	1.354	0.916	-3.728	0.441	-11.05
13	0.475	-175.1	0.564	167.4	0.691	-174.6	0.343	-170.9
14	0.680	35.52	0.566	10.68	0.549	17.43	0.162	171.3
15	0.333	-173.1	0.315	167.1	0.311	-147.8	0.344	6.454
16	0.311	74.26	0.196	46.59	0.192	55.61	0.465	-128.7
17	0.335	168.6	0.238	156.2	0.033	-127.9	0.189	65.30
18	0.199	158.7	0.119	149.4	0.040	118.9	0.150	-44.54

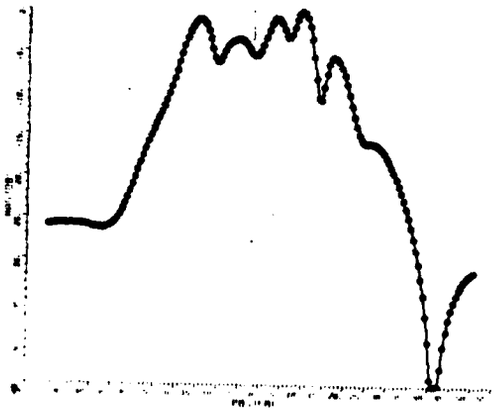

Case I: $\Delta x=0.1\lambda$

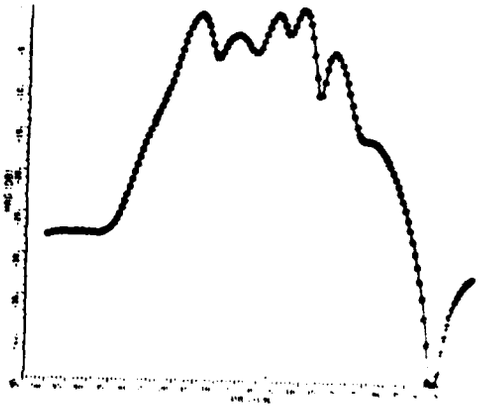

Case III: $\Delta x=0.4\lambda$

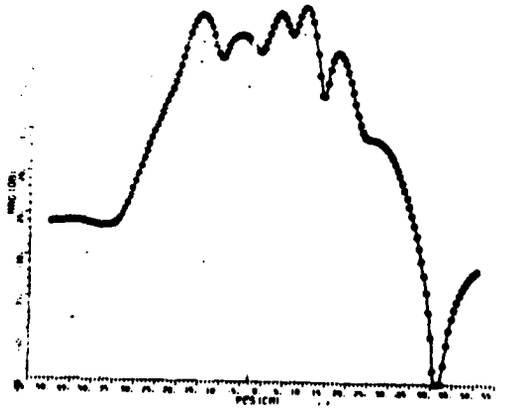

Case II: $\Delta x=0.2\lambda$

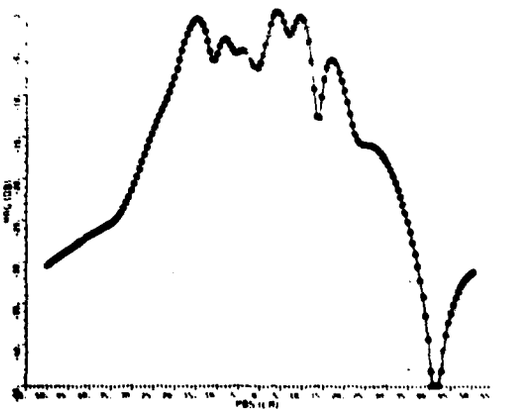

Case IV: $\Delta x=0.8\lambda$

Figure 71: Computed near field magnitude plots corresponding to various measurement sampling distances.

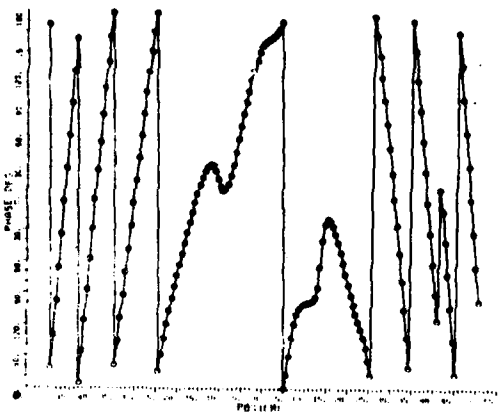

Case I: $\Delta x=0.1\lambda$

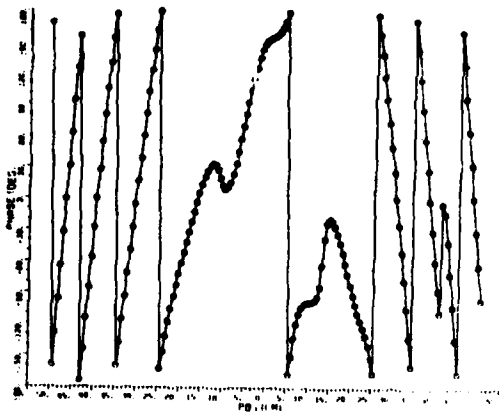

Case III: $\Delta x=0.4\lambda$

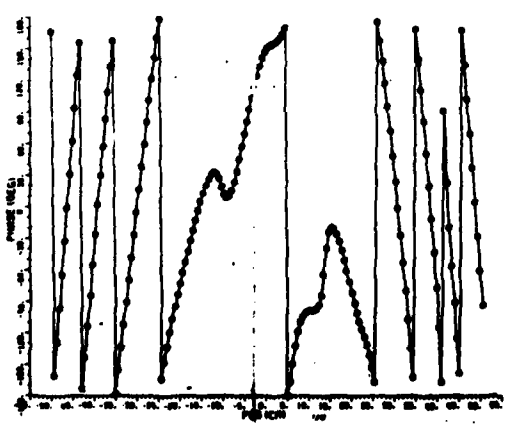

Case II: $\Delta x=0.2\lambda$

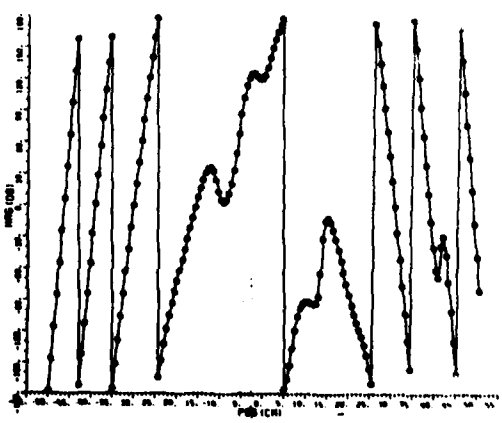

Case IV: $\Delta x=0.8\lambda$

Figure 72: Computed near field phase plots corresponding to various measurement sampling distances.

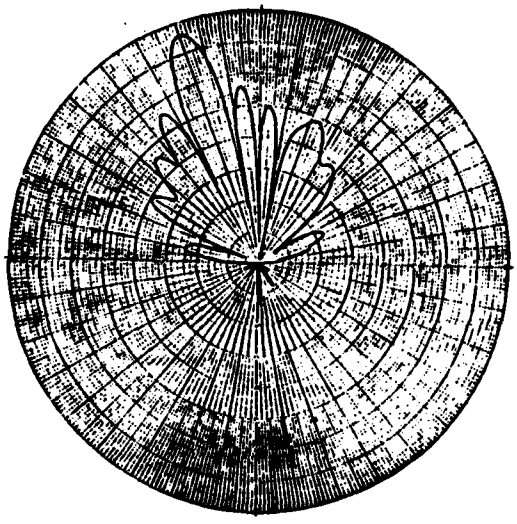

Case I: $\Delta x=0.1\lambda$

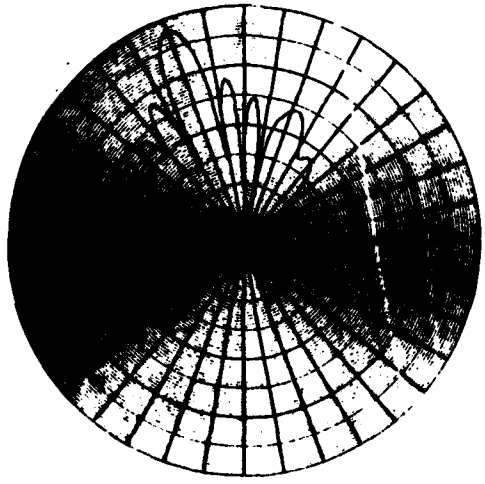

Case III: $\Delta x=0.4\lambda$

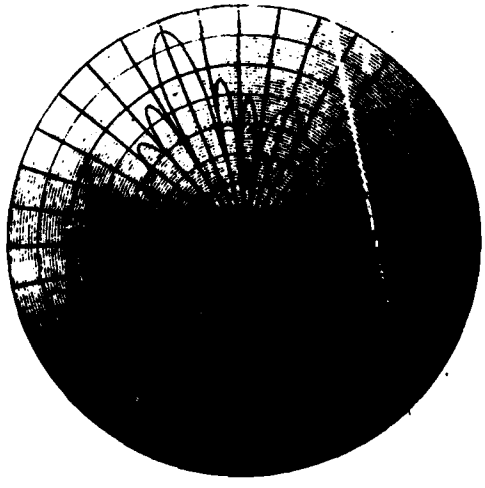

Case II: $\Delta x=0.2\lambda$

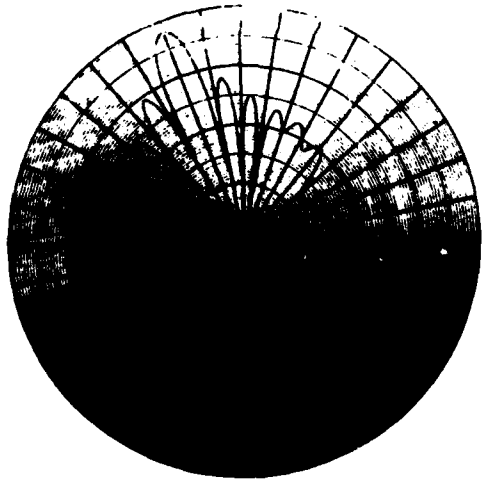

Case IV: $\Delta x=0.8\lambda$

Figure 73: Computed fresnel region plots corresponding to various measurement sampling distances.

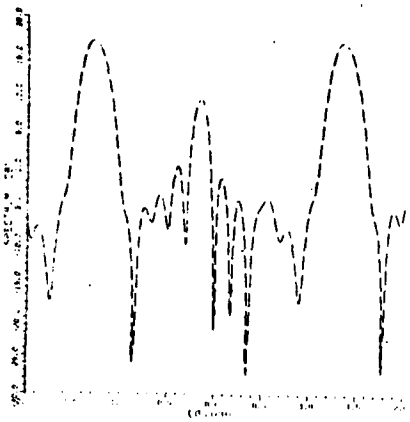

Case I: -50 cm < x < 51 cm

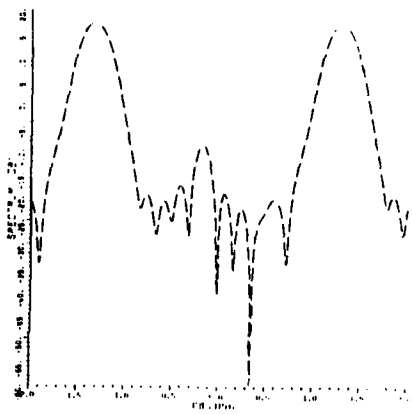

Case III: -25 cm < x < 25 cm

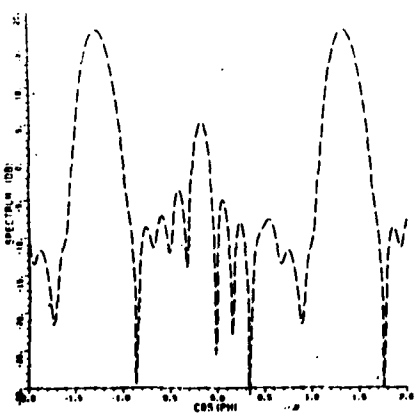

Case II: -37 cm < x < 37 cm

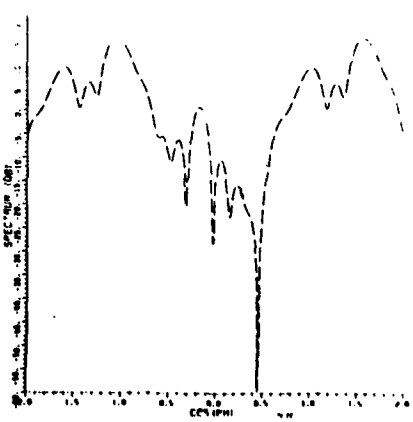

Case IV: -18 cm < x < 18 cm

Figure 74: Computed free space, far field spectrums corresponding to various ranges of near field measurements.

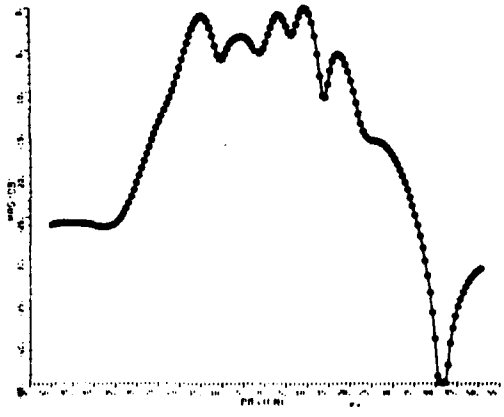

Case I: -50 cm < x < 51 cm

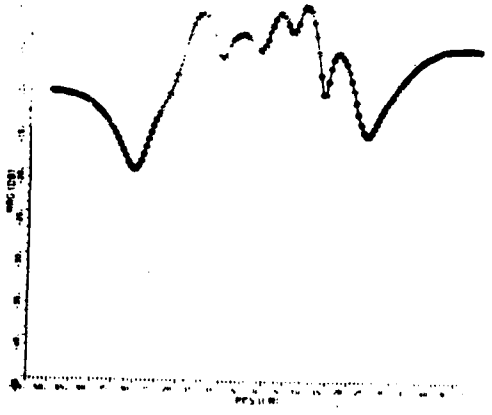

Case III: -25 cm < x < 25 cm

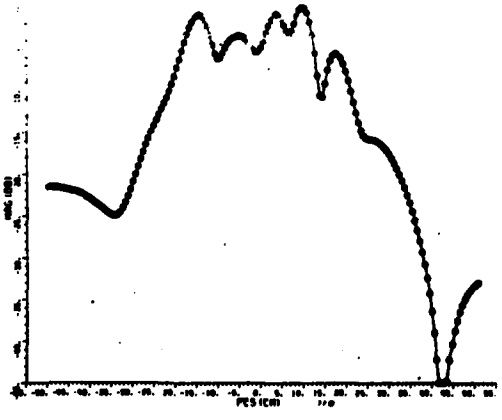

Case II: -37 cm < x < 37 cm

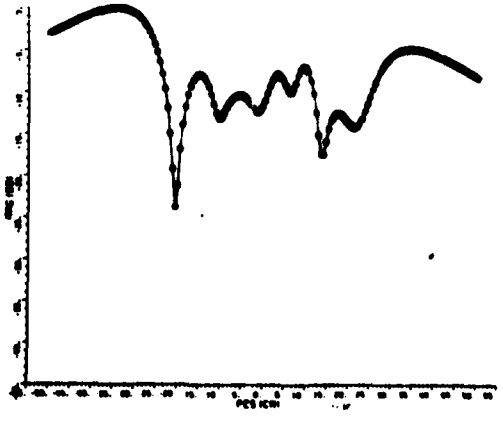

Case IV: -18 cm < x < 18 cm

Figure 75: Computed near field magnitude plots corresponding to various ranges of near field measurements.

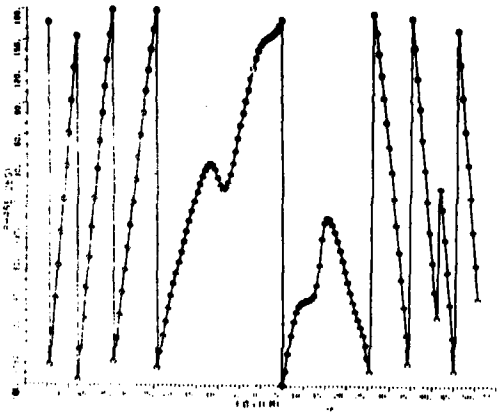

Case I: -50 cm < x < 51 cm

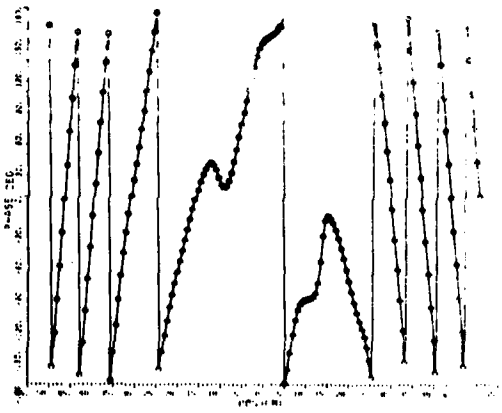

Case III: -25 cm < x < 25 cm

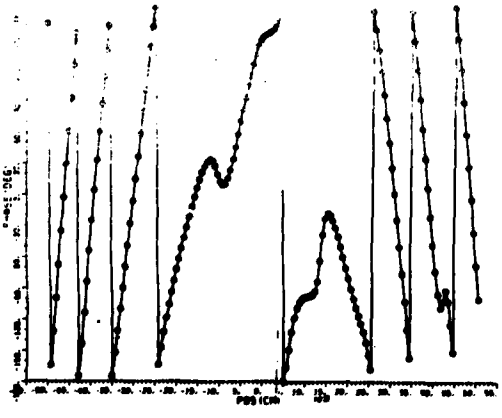

Case II: -37 cm < x < 37 cm

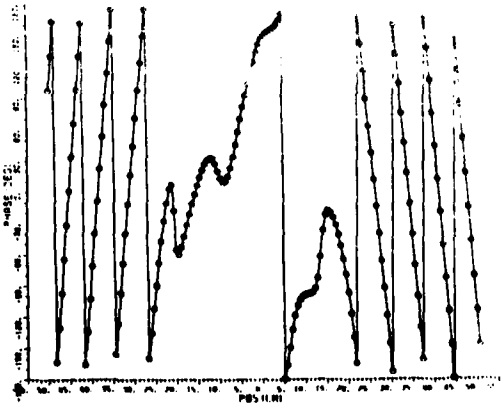

Case IV: -18 cm < x < 18 cm

Figure 76 : Computed near field phase plots corresponding to various ranges of near field measurements.

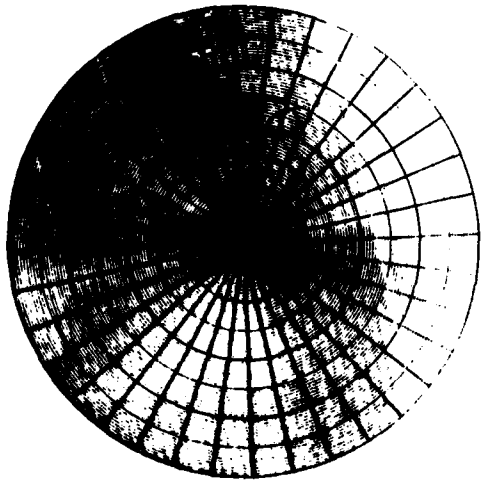

Case I: -50 cm < x < 51 cm

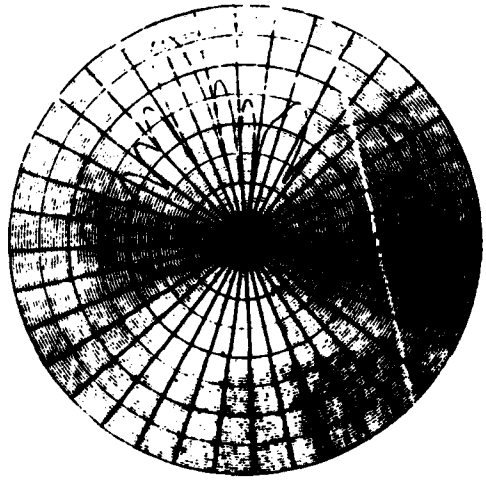

Case III: -25 cm < x < 25 cm

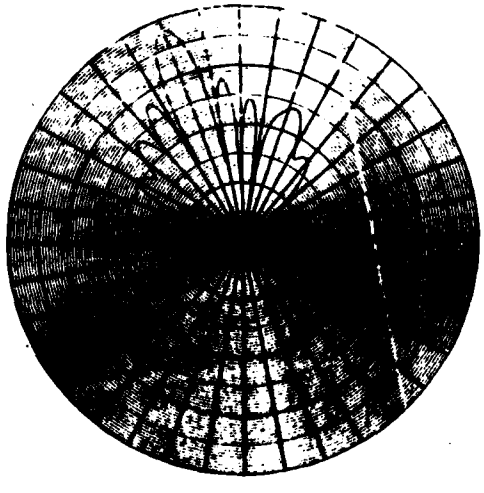

Case II: -37 cm < x < 37 cm

Case IV: -18 cm < x < 18 cm

Figure 77: Computed fresnel region plots corresponding to various ranges of near field measurements.

is greatly affected by the measurement range. Thus,the measurement range necessary to obtain a meaningful solution must be great enough to include a significant portion of the radiated energy of a pattern cut.

SECTION X

APPLICATION OF DETERMINED CURRENTS IN GTD COMPUTER CODES

A. INTRODUCTION

As previously discussed the main goal of this method is to determine the source distributions or current solutions of array antennas for use in GTD computer codes. This permits the source to be accurately modelled in the GTD computer codes. These codes can then be used to calculate the pattern characteristics of antenna arrays placed in various surroundings of scatterers. The Basic Scattering Code[7][10][11] which was used in conjunction with determining the currents is also ideal for many of these field calculations. In an effort to more clearly demonstrate the advantages of having antenna source information as obtained through the procedures described in this report, far field pattern calculations are effected for the antenna array of figure 1 with metallic scatterers nearby. More specifically, these pattern calculations are done first with a large cylindrical scatterer placed at various positions in front of the antenna and then with a plate scatterer placed above the array. These objects could represent a mast of a ship and an aircraft wing. Without knowledge of these element excitations the effect of these scatterers on the antenna patterns could only be aquired through extensive measurements. This procedure is normally expensive. Sometimes, the effect of nearby scatterers can be ascertained through pattern calculations with source assumptions but normally this has the disadvantage that important pattern characteristics might be unaccounted for.

B. EFFECT OF CYLINDRICAL SCATTERER ON FAR FIELD ANTENNA PATTERN

The geometry of the antenna, ground plane, and cylinder is shown in figure 78. Eight cases were considered in which the parameters R and ϕ were varied. The radial parameter, R, was set at 10λ and 5.7λ, and the ϕ parameter was varied through 18^0,28^0,38^0, and 58^0. These cases are listed in table 19. Figures 81 through 88 show azimuth E_z far field plots corresponding to the cases of Table 19. Free space far field plots of the antenna and ground plane are shown in figures 79 and 80 for comparison. As seen in the plots for the $R=5.7\lambda$ case principal sidelobe distortion is just noticeable at $\phi=28^0$ and main lobe distortion is present at $\phi=38^0$. The $R=10\lambda$ cases, however, show that principal

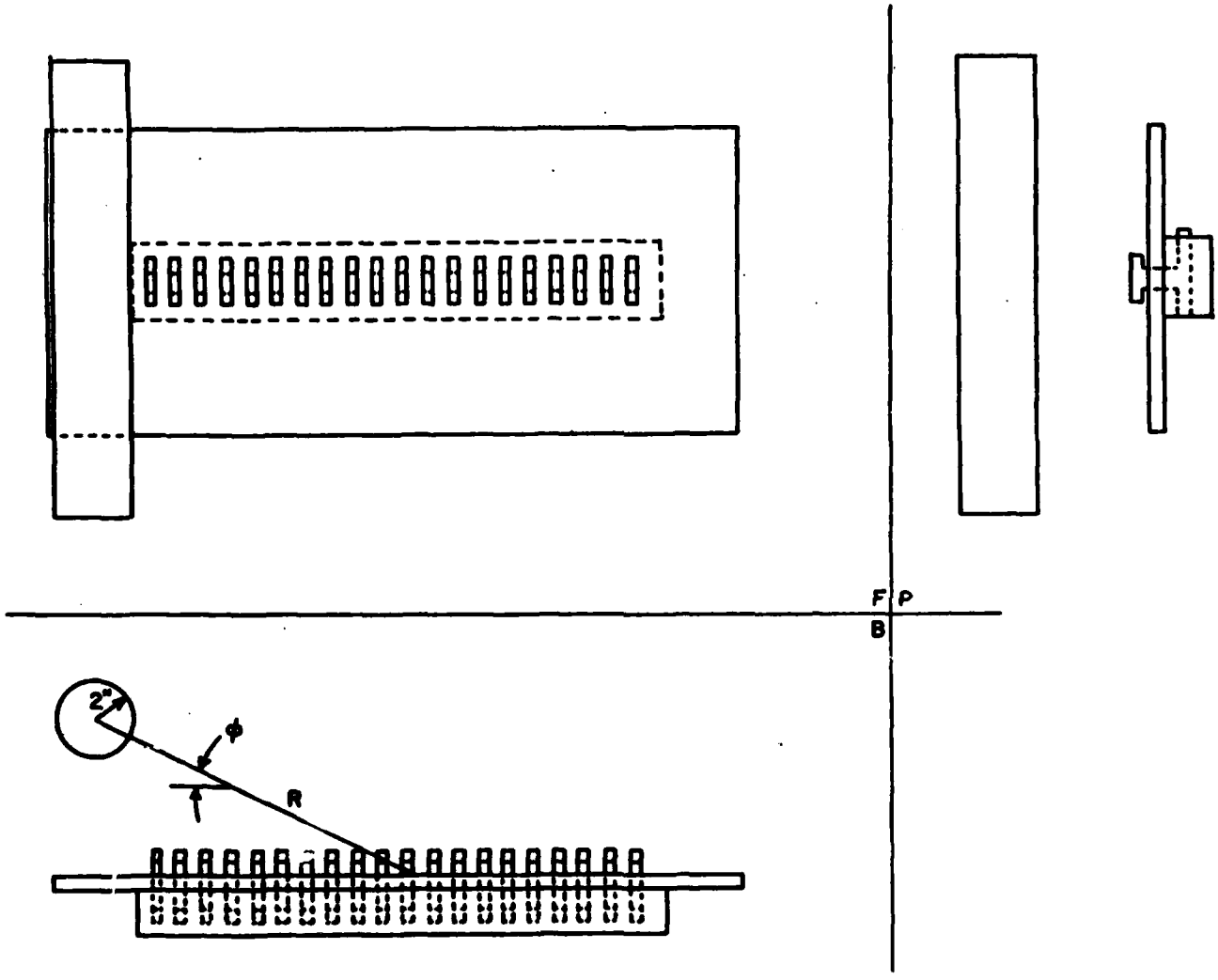

Figure 78: Geometry of antenna, ground plane, and cylinder.

TABLE 19

SUMMARY OF CYLINDER POSITIONS FOR R=5.7λ AND R=10λ

CASE #	RADIUS	ϕ (DEGREES)
1	5.7λ	18°
2	5.7λ	28°
3	5.7λ	38°
4	5.7λ	58°
5	10λ	18°
6	10λ	28°
7	10λ	38°
8	10λ	58°

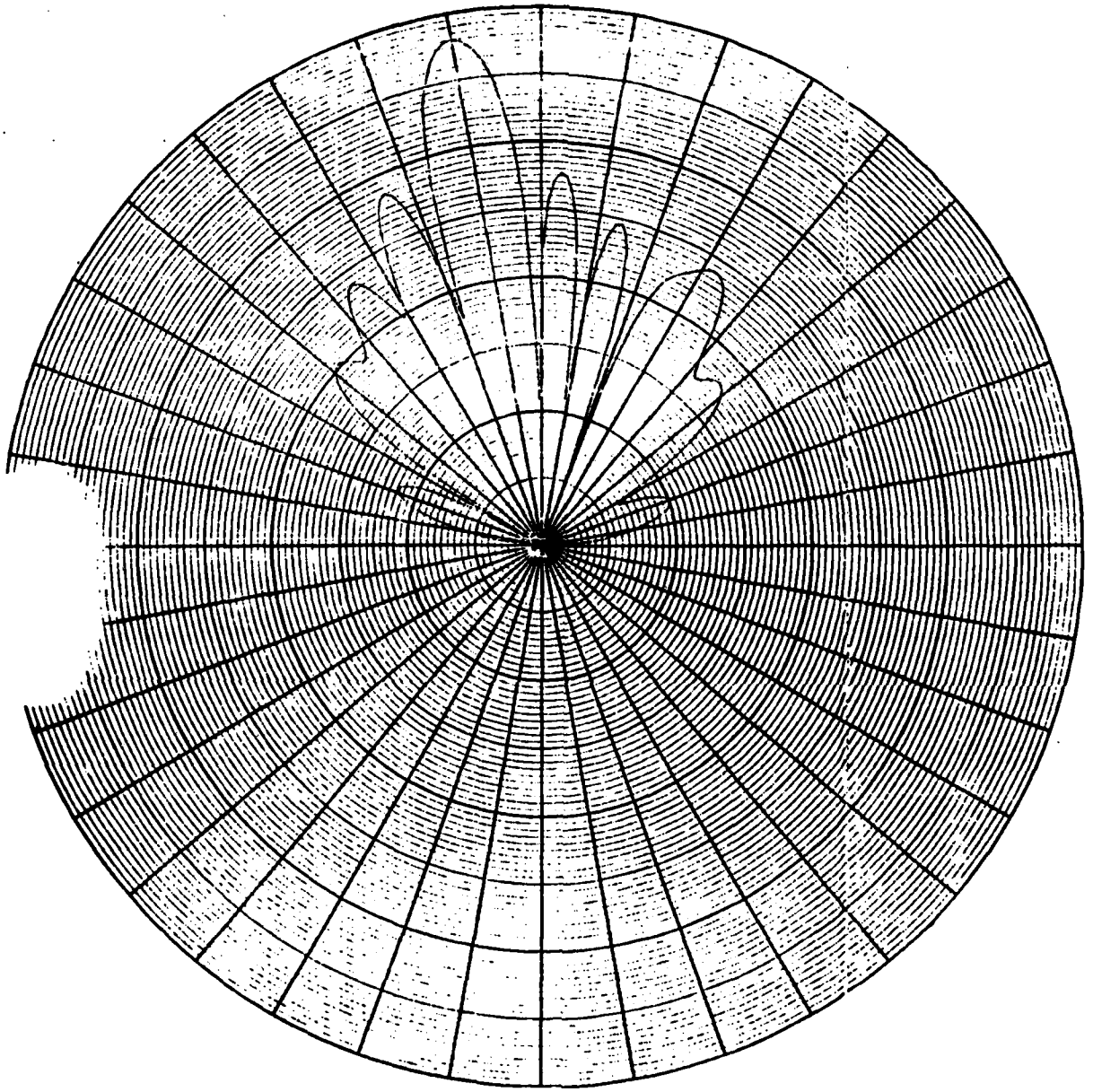

Figure 79: Free space, far field (horizontal cut) of antenna and ground plane.

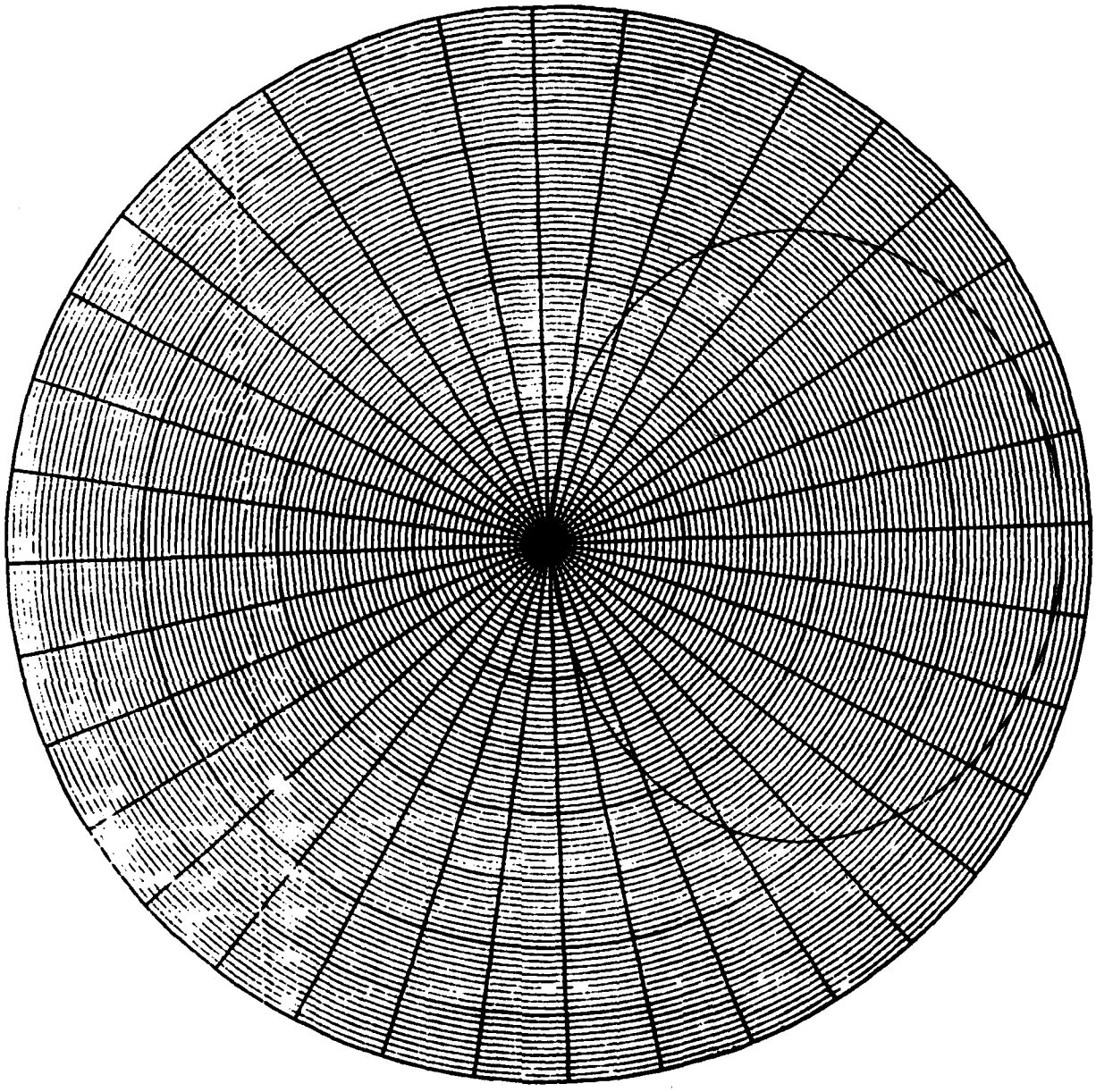

Figure 80: Free space, far field (elevation cut) of antenna and ground plane.

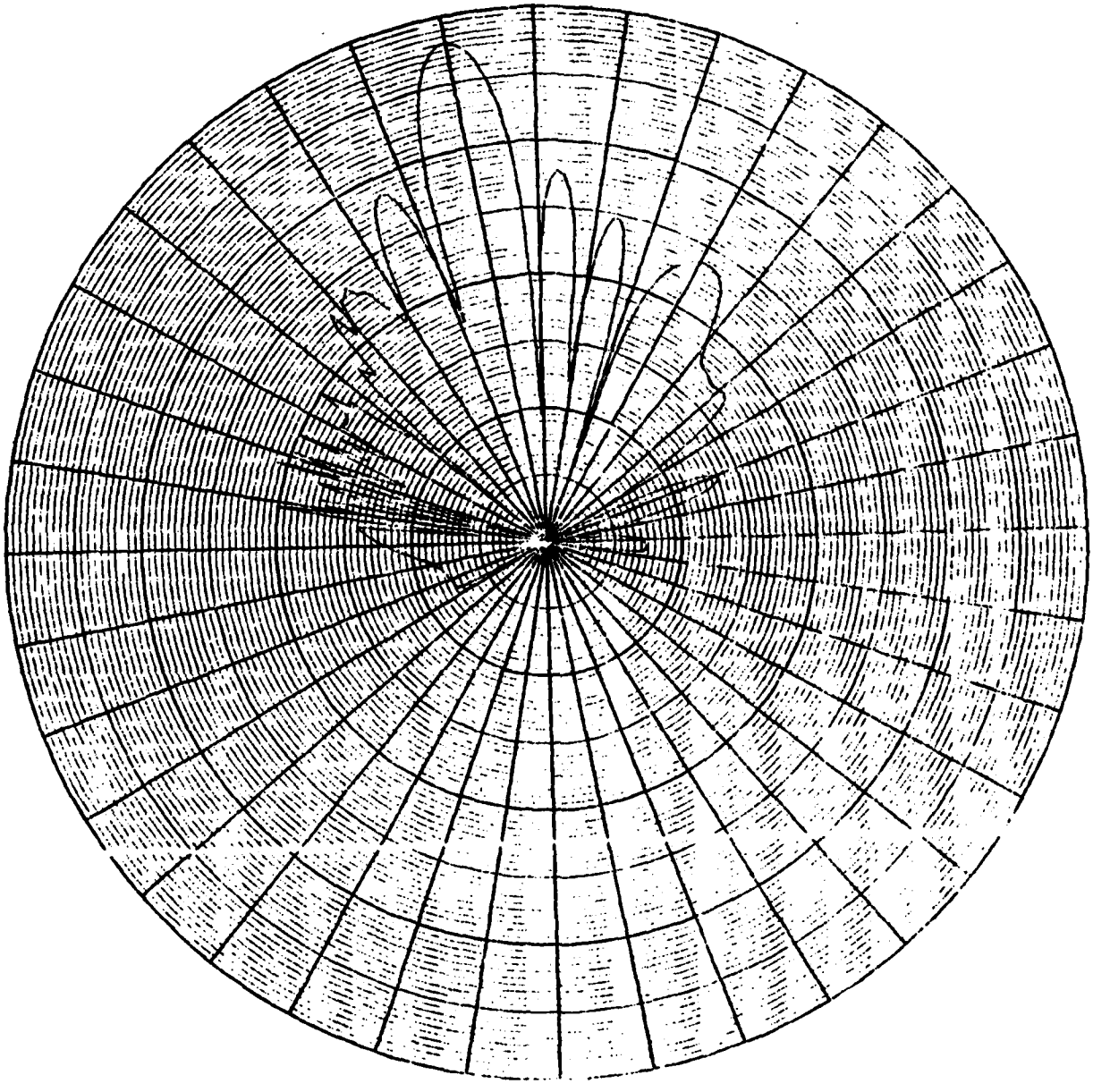

Figure 81: Far field, horizontal pattern corresponding to case 1 of table 19.

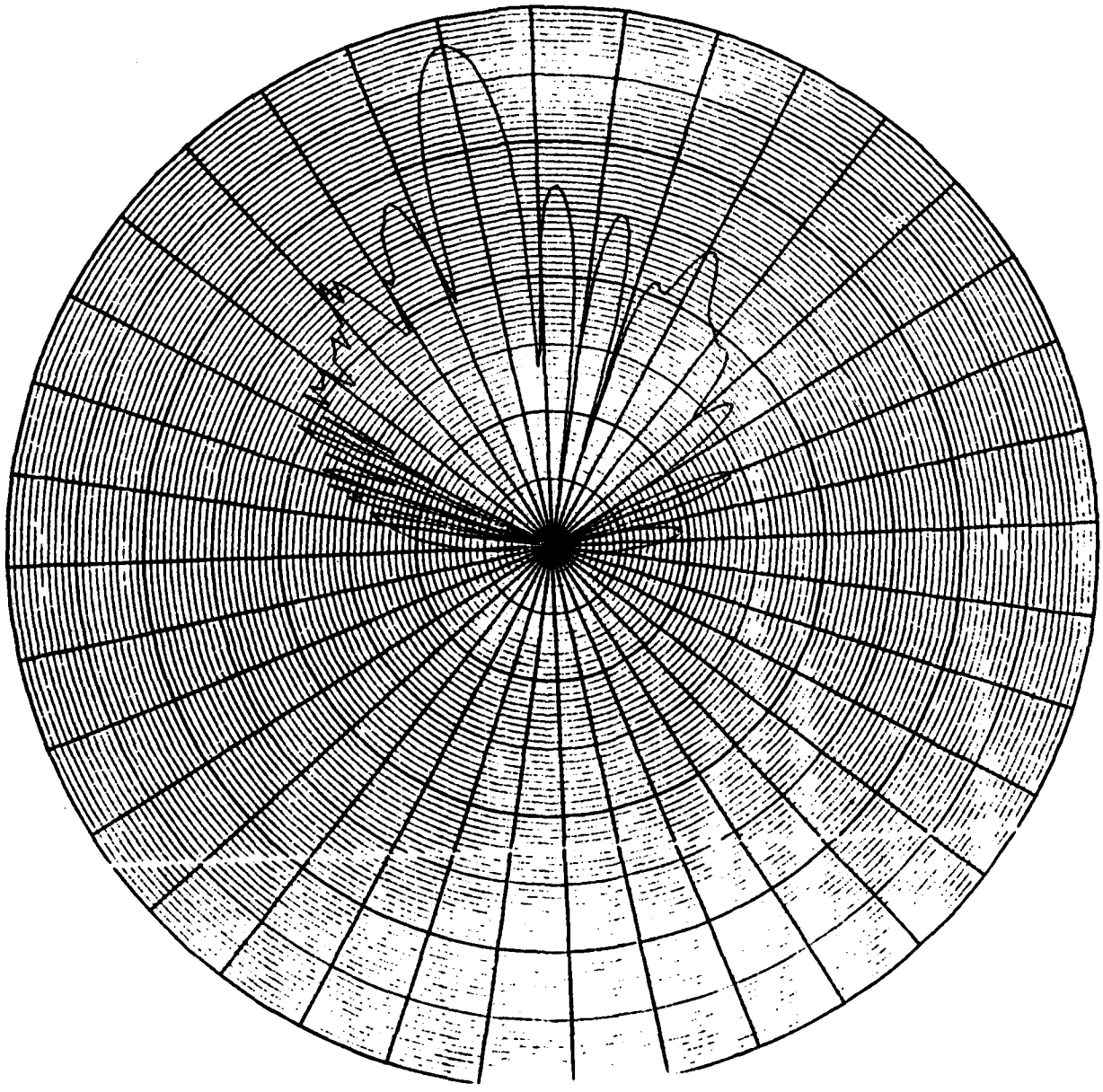

Figure 82: Far field, horizontal pattern corresponding to case 2 of table 19.

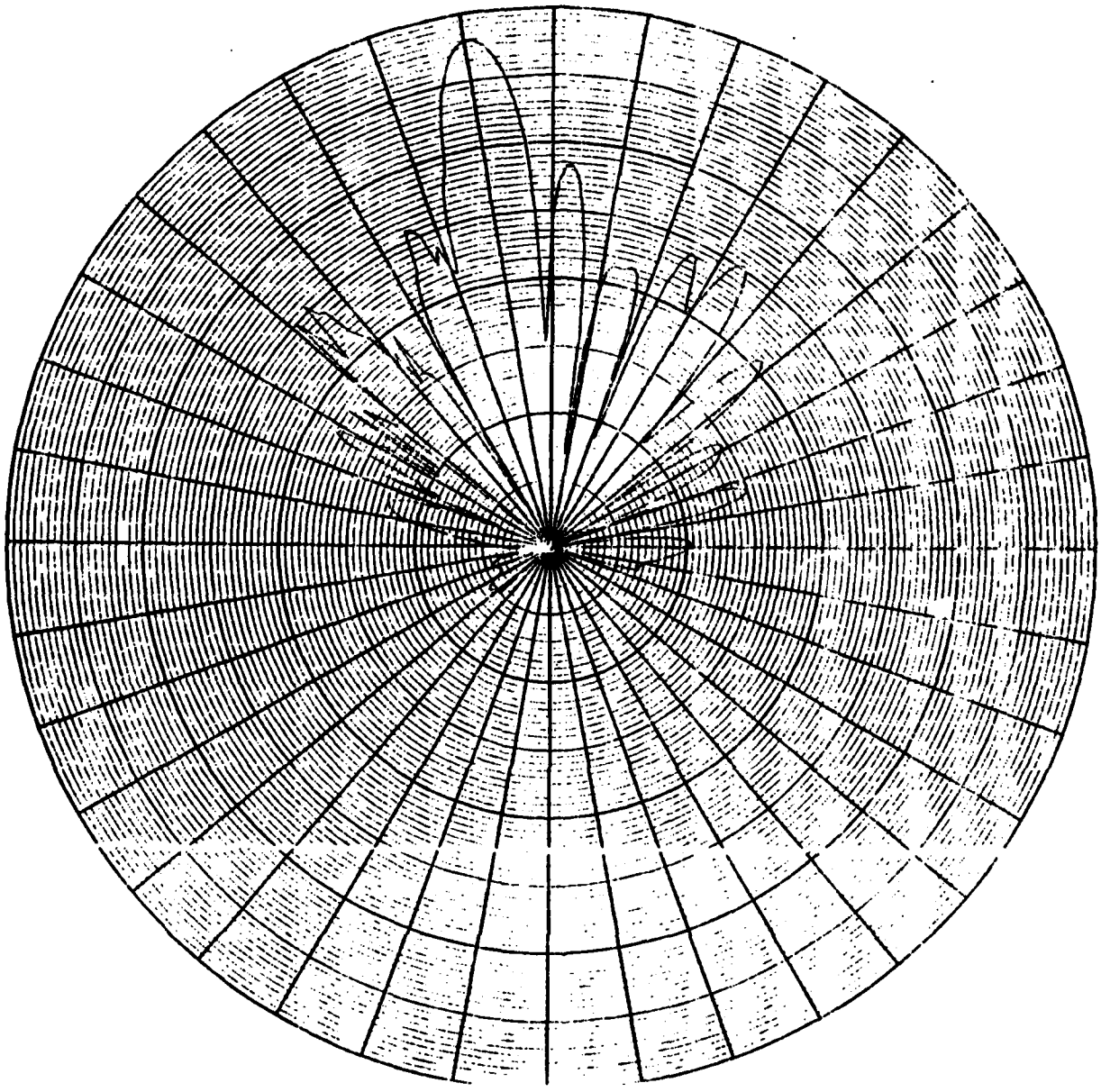

Figure 83: Far field, horizontal pattern corresponding to case 3 of table 19.

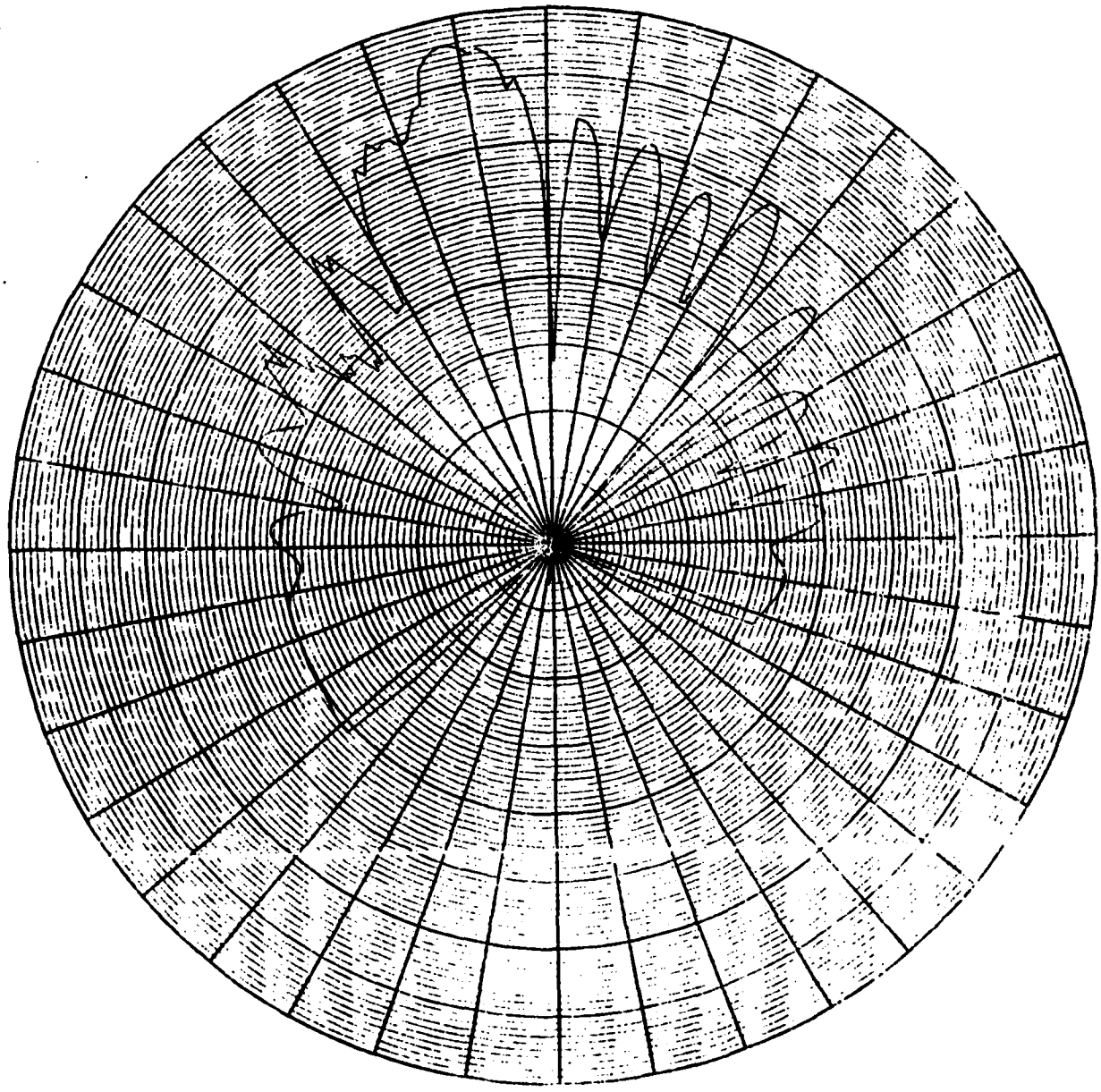

Figure 84: Far field, horizontal pattern corresponding to case 4 of table 19.

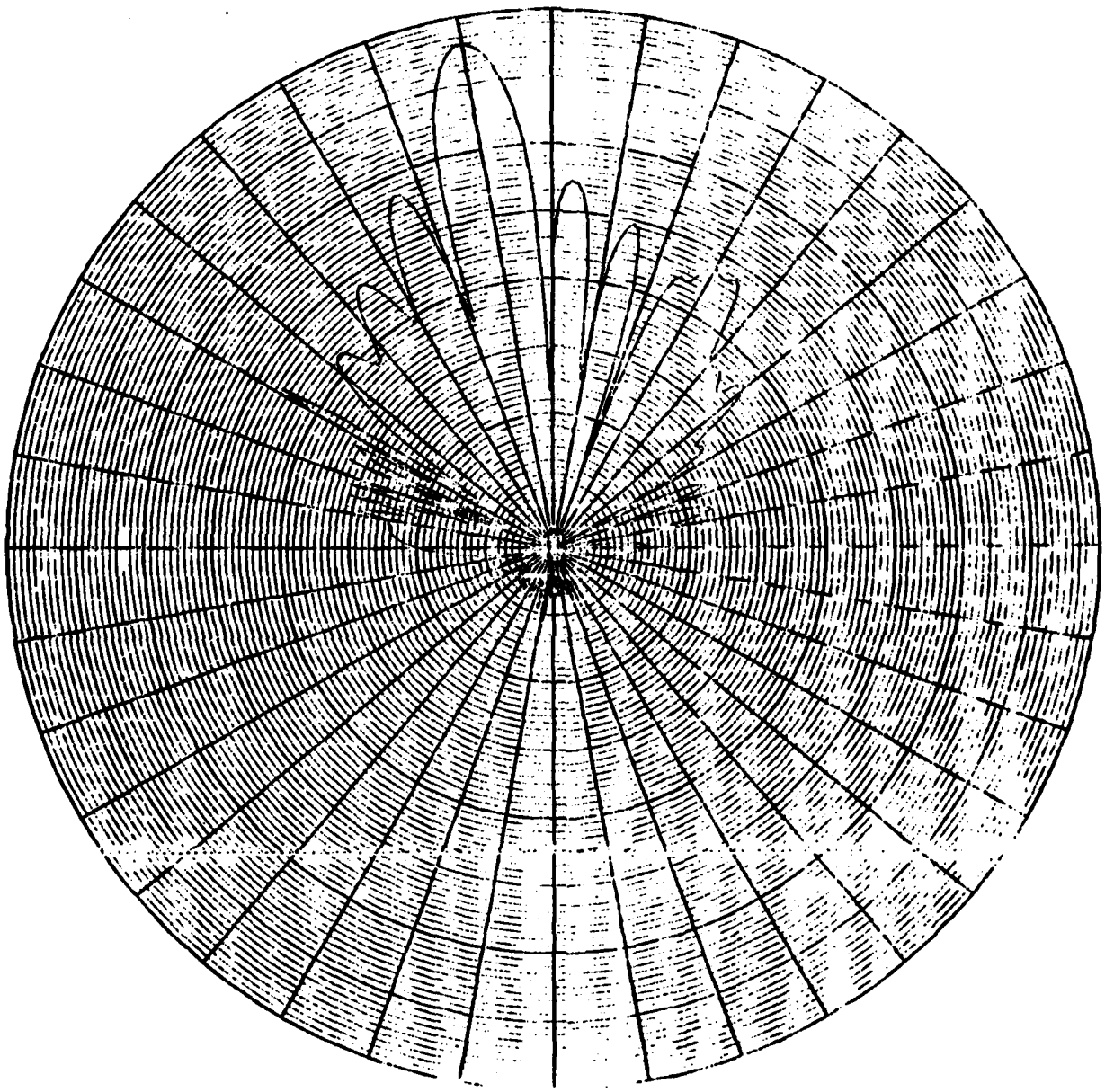

Figure 85: Far field, horizontal pattern corresponding to case 5 of table 19.

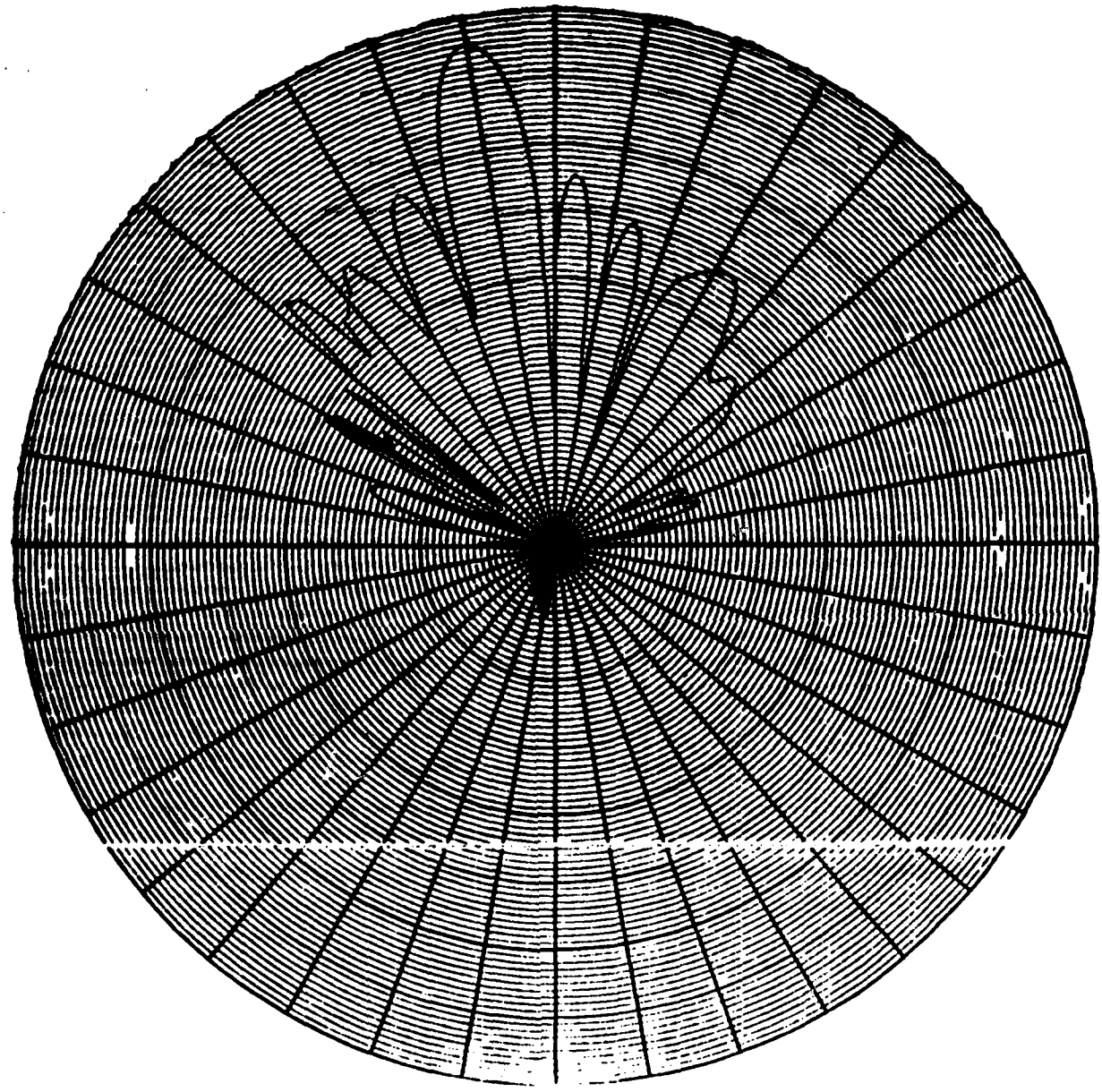

Figure 86: Far field, horizontal pattern corresponding to case 6 of table 19.

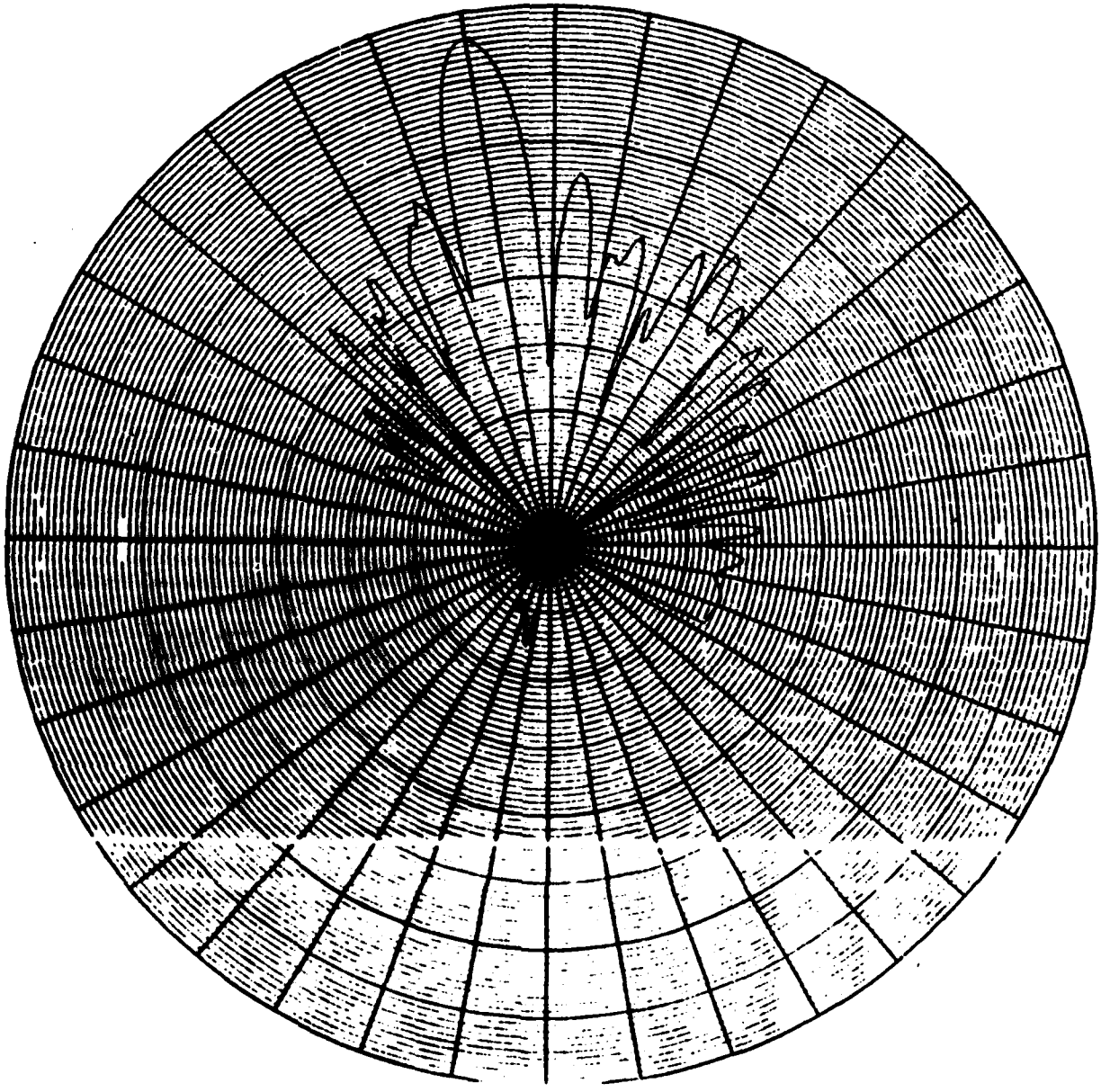

Figure 87: Far field, horizontal pattern corresponding to case 7 of table 19.

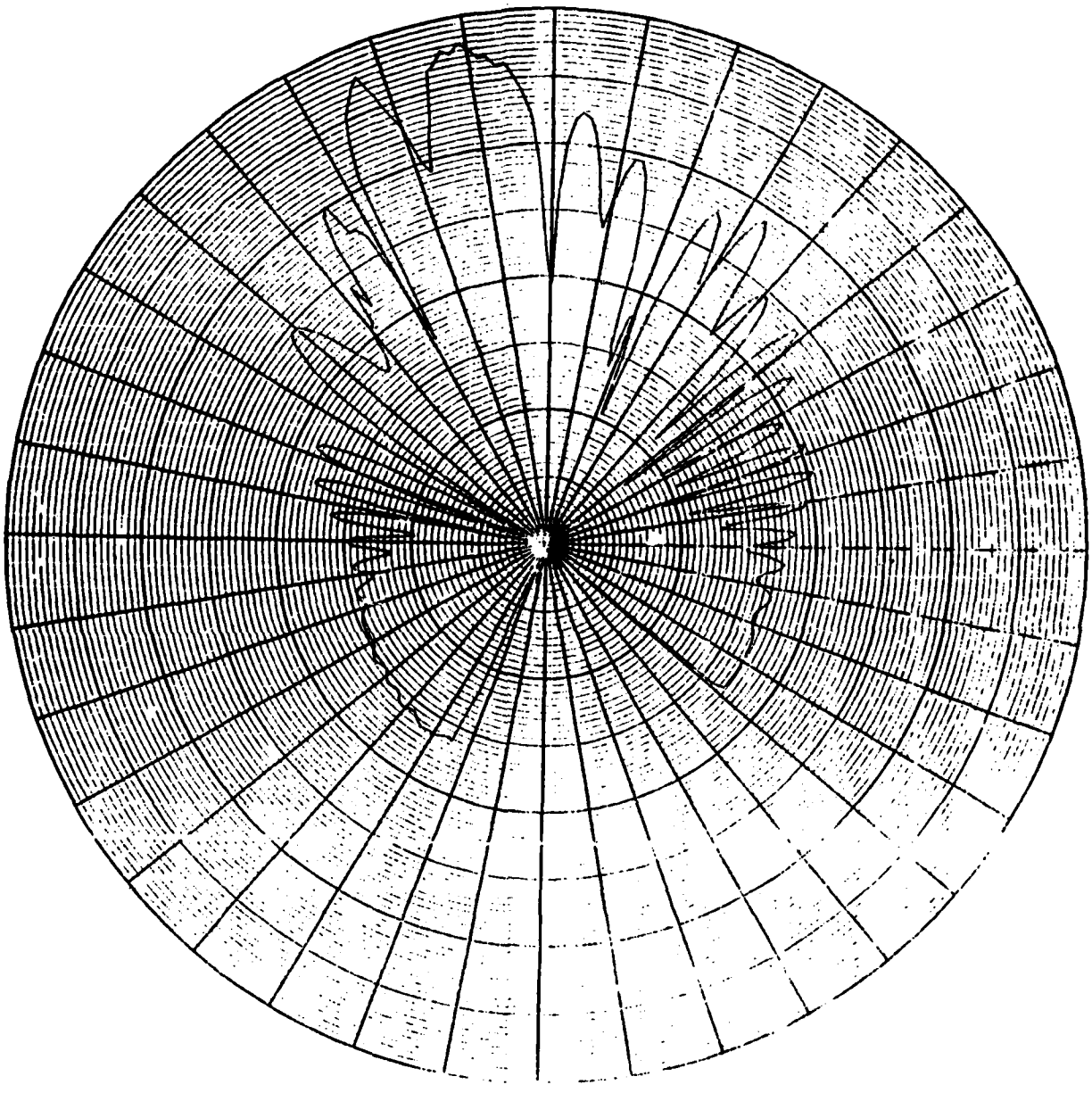

Figure 88: Far field, horizontal pattern corresponding to case 8 of table 19.

sidelobe distortion is noticeable at $\phi=38^0$ and the main lobe is distorted at $\phi=58^0$.

C. EFFECT OF PLATE SCATTERER ON FAR FIELD ANTENNA PATTERN

The geometry of the antennna, ground plane, and plate is shown in figures 89. The parameter varied in this case was the d parameters of the plate postion. Two cases are considered. In the first case the plate center is at $d=0\lambda$ and in the second the plate center is at $d=19\lambda$. These cases are summarized in table 20. Both azimuth and elevation far field pattern cuts were computed and these are shown in figures 90 through 93. Figures 79 and 80 show azimuth and elevation far field pattern cuts of the antenna in free space for comparision. It turns out that the azimuth patterns were not greatly affected by the plate. The principal sidelobes showed slight distortion and the main lobe showed none. The elevation cut, however was significally affected, especially for case 1 with d=0 as shown in Figure 89.

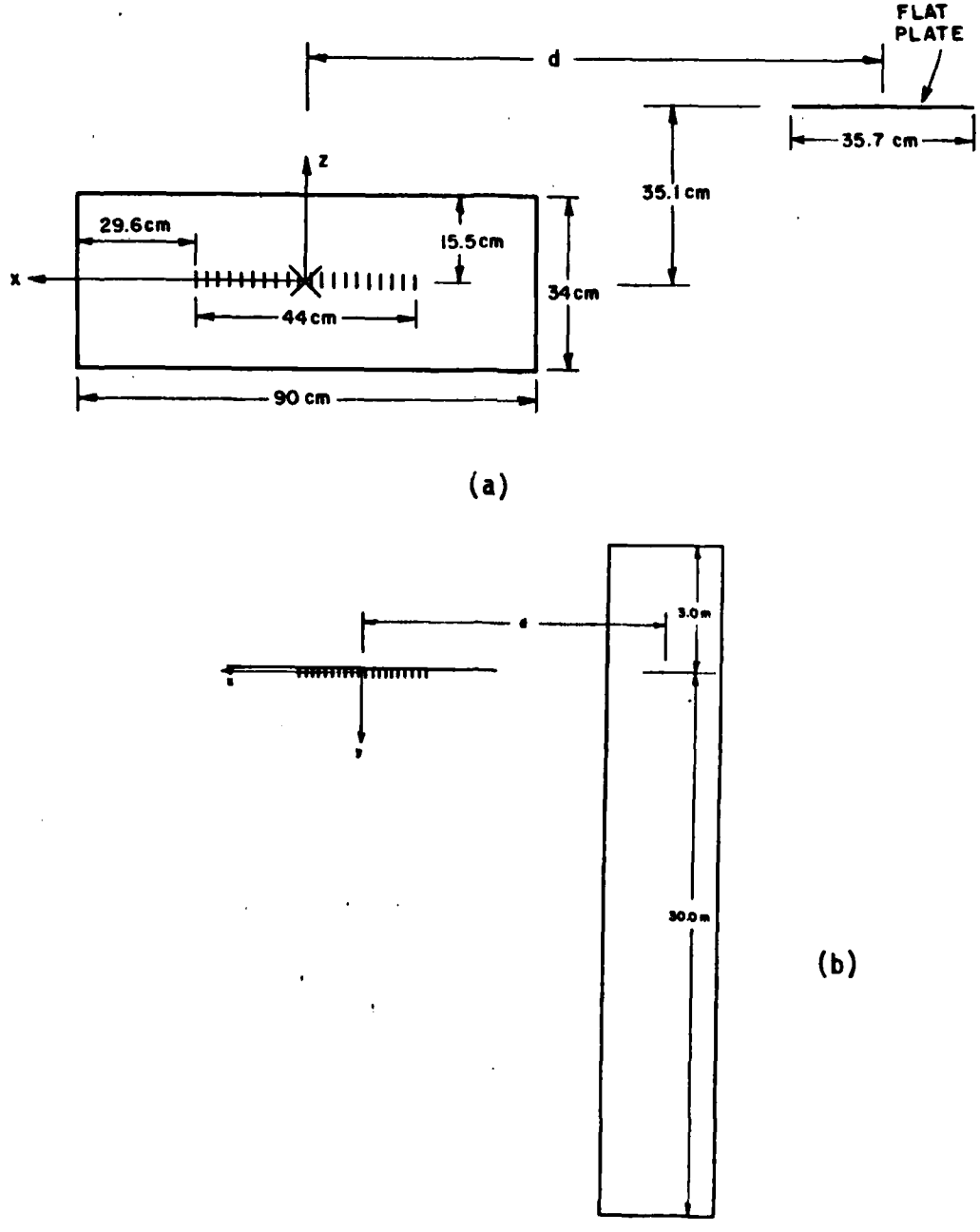

Figure 89: (a) Front view of geometry of antenna, ground plane, and plate.

(b) Top view of geometry of antenna, ground plane, and plate.

TABLE 20

SUMMARY OF PLATE POSITIONS AS REFERENCED TO FIGURE 81

CASE #	d (WAVELENGTHS)
1	0
2	19

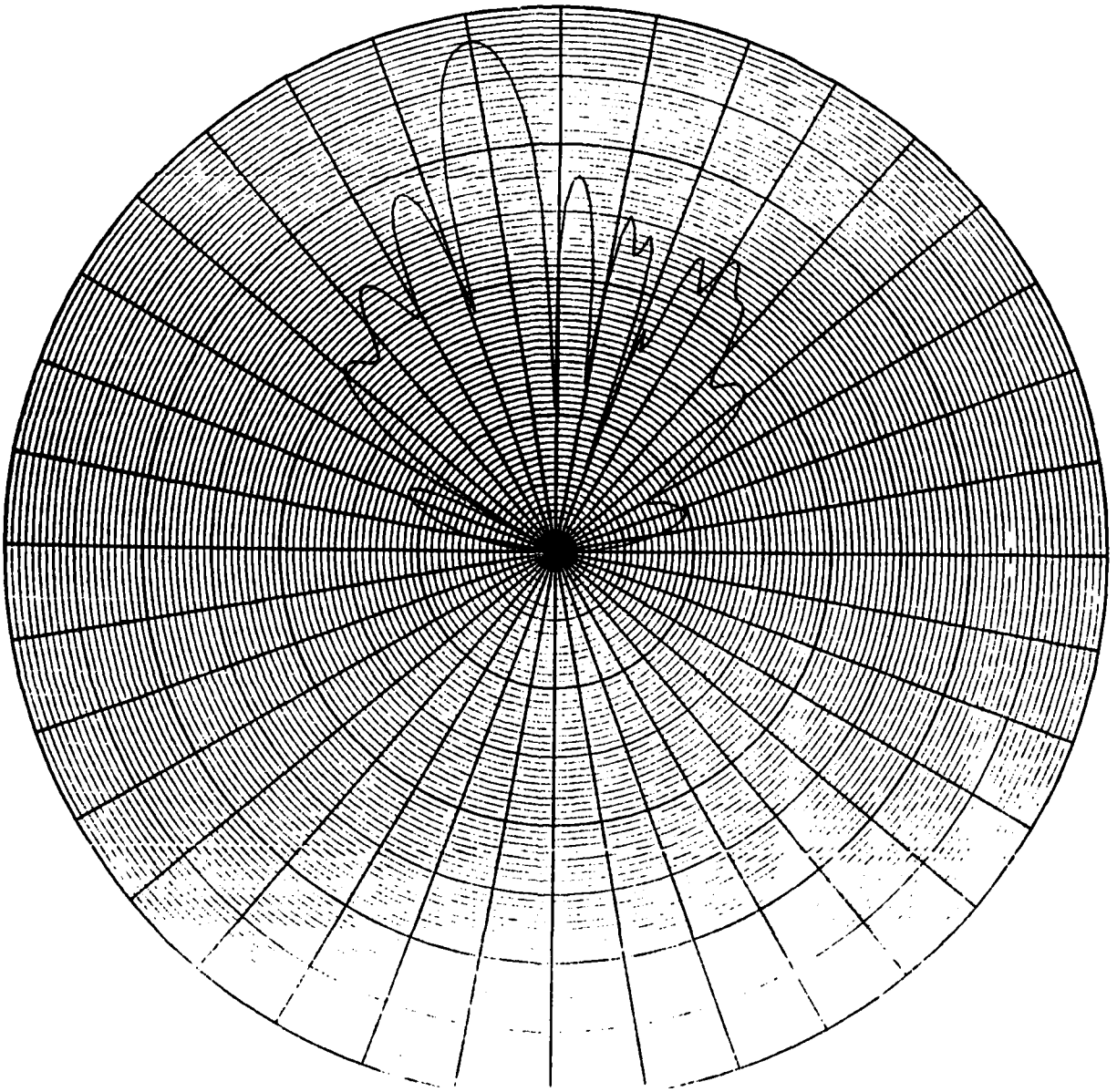

Figure 90: Far field horizontal pattern corresponding to case 1 of table 20.

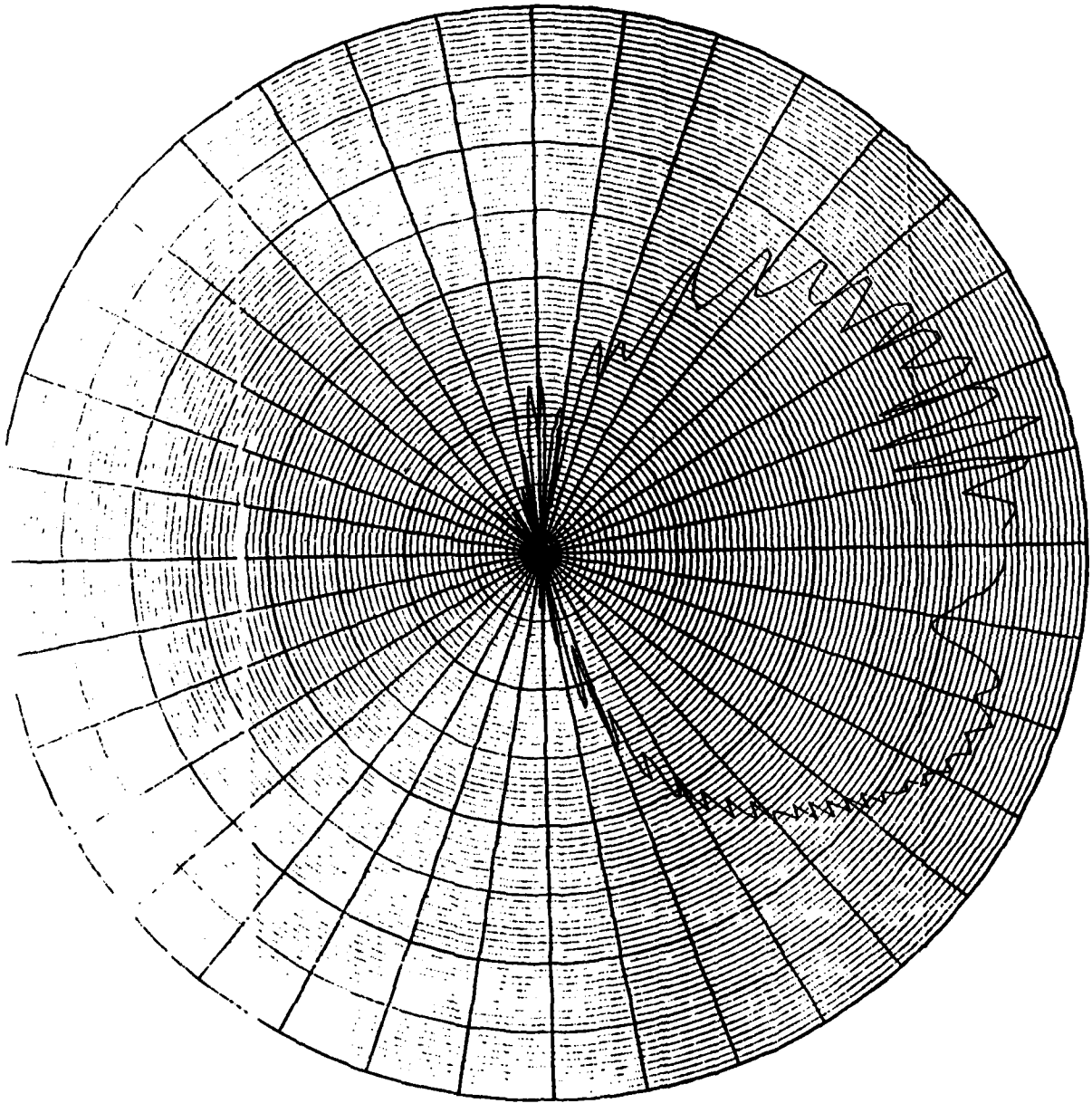

Figure 91: Far field elevation pattern corresponding to case 1 of table 20.

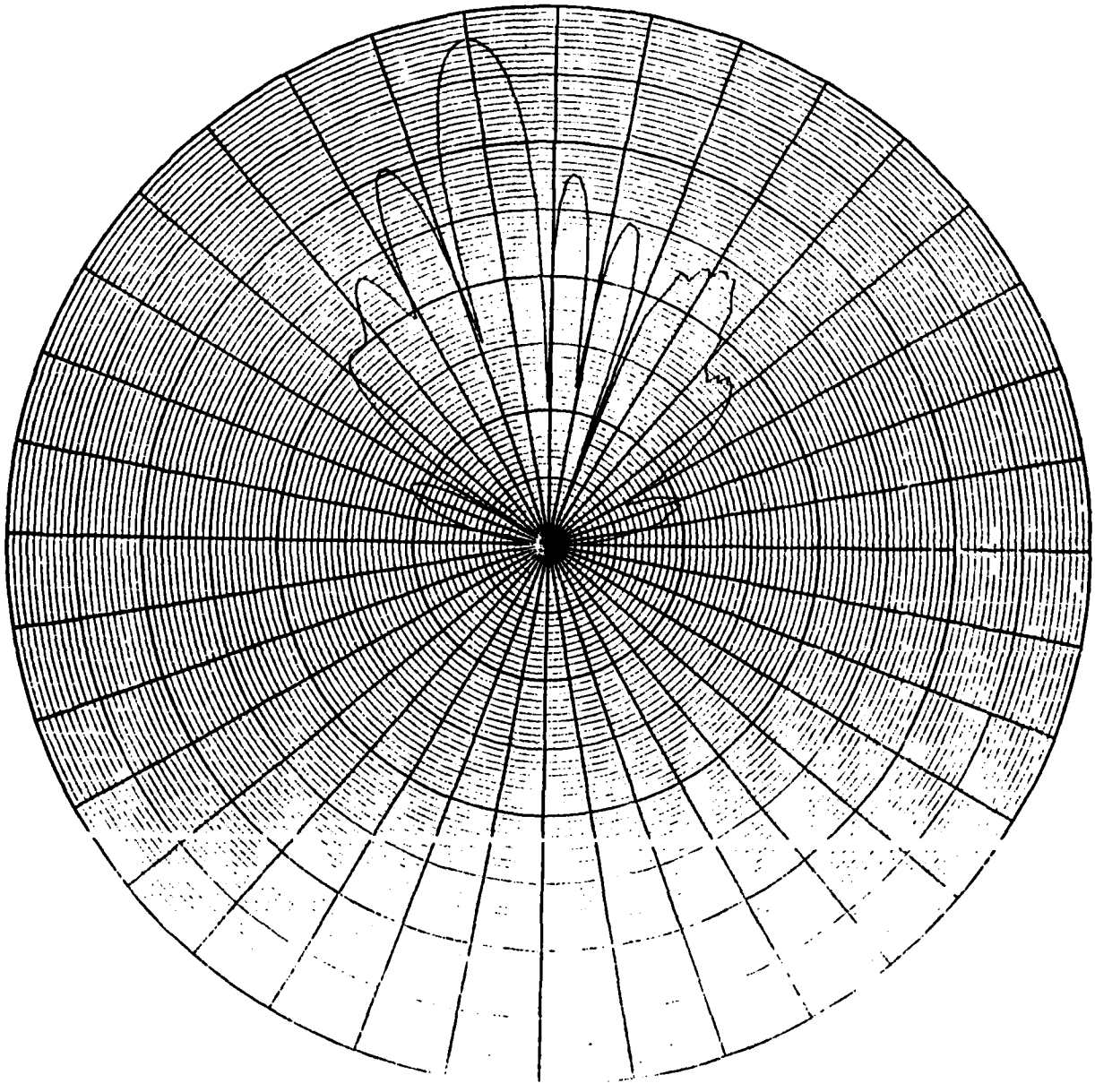

Figure 92: Far field horizontal pattern corresponding to case 2 of table 20.

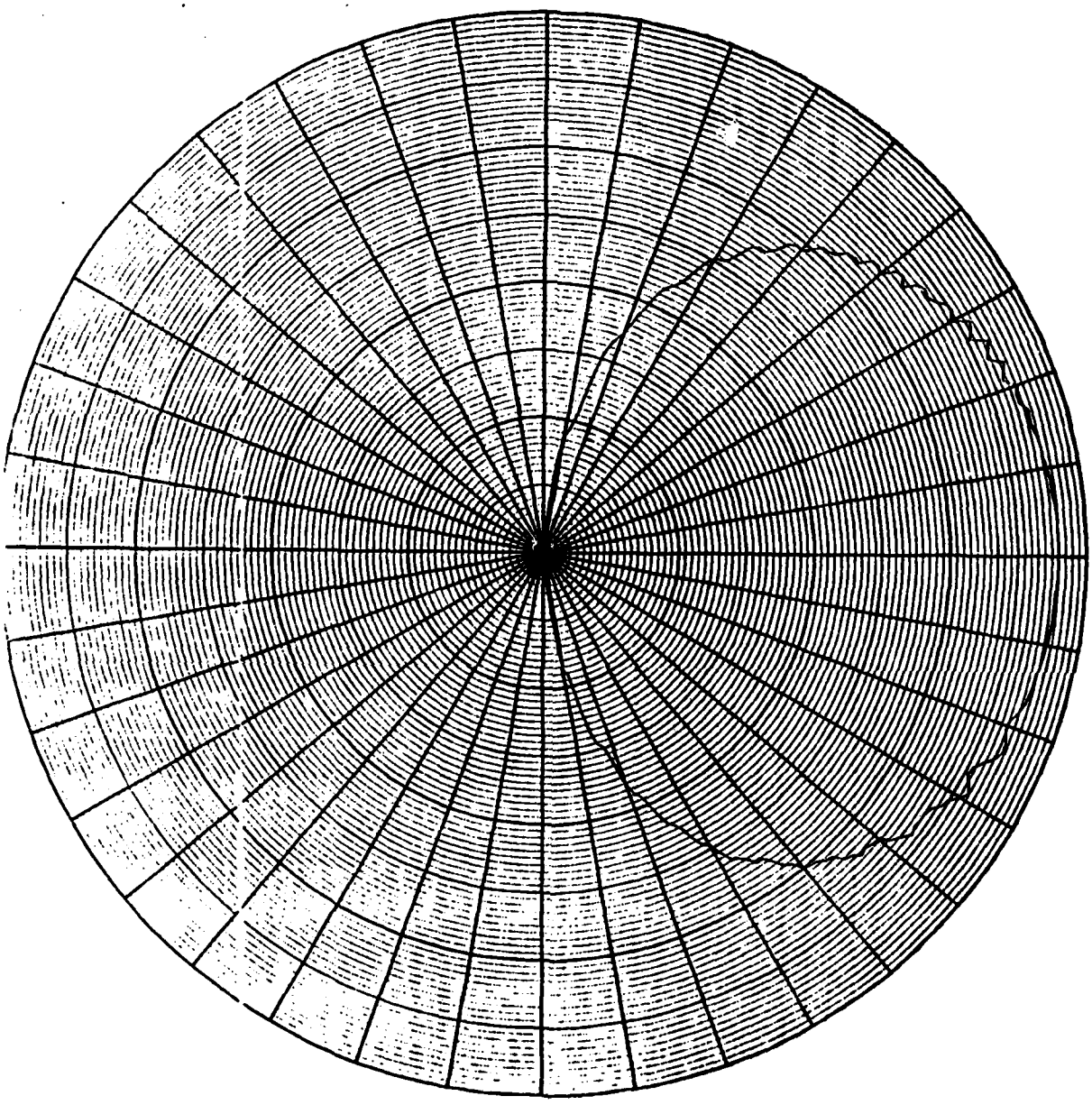

Figure 93: Far field elevation pattern corresponding to case 2 of table 20.

SECTION XI

SUMMARY, CONCLUSION, AND FUTURE WORK

A. SUMMARY

In this thesis a synthesis technique was applied to determine array excitations from measured near field data with promising success. Unlike in synthesis where the task is to find a source distribution which radiates a field similar to the desired field, the task here was to find the set of currents which existed on an array using measured near field data. This was accomplished, in part at least, through relating discrete point currents of the array to a measured, radiated near field in an overconstrained matrix equation and solving for the excitations. The solution was carried out both with and without an imposed source euclidean norm constraint. It was thought that the constraint was needed since different unconstrained currents resulting from different near field data of different measurement pattern cuts was inconsistent and all solutions were unrealistically highly reactive. It turns out that reducing the source norm is equivalent to reducing the solution reactivity. The imposition of source norm constraint, however, increases the euclidean error between the computed near field of the solution and the measured near field. The amount of constraint imposed in the solution process was decided through a trial and error process which involved subjective correlation of measured and computed radiatied fields, examination of free space far field plots which showed invisible as well as visible regions, and examination of the current phase distribution which, through aprori knowledge, was expected to be linear. A variation of this technique was also, attempted in which only near field magnitude quantities were specified while various initial measurement phase distributions were assumed and a phase iteration process was applied. This procedure failed to converge to currents which could produce measured near and Fresnel region fields. Even though the phase is needed, it is relatively easy to obtain in the near field as shown here.

Four near field measurements were made on the array with 169 magnitude and phase data points acquired from each measurement session. The last was made after it was discovered that a cable problem had changed the current distribution of the array between the near field and Fresnel field measurements which resulted in degraded correlation between computed and measured Fresnel plots. The measurements were made

by moving a probe along a line parallel to and in the H-plane of the array. Each measurement set was taken with the line of measurement displaced a different distance from the array. The measurement spanned approximately 8λ to each side of the center of the array and the component of the electric field aligned with the array dipoles was measured with a balanced dipole probe. The measurement design was such that the probe was always in the far field of any individual array element. Also the measurement axis was perpendicular to the dipoles so that the elememt factor of the array elements and the probe was of the same value at every measurement point.

The resultant unconstrained currents corresponding to the initial three measured data sets using both measured magnitude and phase samples were unrealistically reactive and showed little consistency as mentioned above. Examination of the free space, far field spectrums revealed that the visible regions of these curves were similar and the invisible regions were different, thus, indicating that each solution represented a different degree of reactivity. The near fields computed from these currents correlated well with the measurements. Fresnel region comparisons were less than expected though and this was found to be due to a cable problem which occured between near field and Fresnel field measurements. Currents of constrained source norm were computed and these where both of reasonable reactivity and correlated well. Also, the current phase distributions were approximately linear as expected. However, the computed radiated fields of the constrained solutions deviated from those of the unconstrained solutions in the low level and wide angle regions. It was then thought that these currents might be overconstrained and a less constrained, slightly more reactive solution could be found which was realistic yet had radiated fields which correlated well with measurements. This was not pursued with these cases, but rather, the technique was applied to the fourth set of measurements.

Both constrained and unconstrained currents were computed from the fourth set of near field measurements. A constraint was found which resulted in currents of reasonable reactivity and of approximately linear phase. Also, the near and Fresnel radiated fields correlated extremely well with measurements. In addition the solution process was repeated to include the outer four array elements which were not directly excited, but rather, they had only induced currents due to the fields of the other elements. This confirmed the previous assumption that the induced passive currents were small compared to the active currents. The contribution of these additional currents to the computed radiated fields was insignificant and barely noticeable only in the outermost low level regions. Again a constraint was found which resulted in a solution of low reactivity, linear phase, and good correlation between measured and computed fields. The experiences associated with finding constraints for solutions of the fourth data set resulted in a potential algorithm which would allow one to obtain a best

tradeoff between a nonreactive solution and a solution which would have good correlation between computed and measured fields. This algorithm results in a solution which reproduces measured fields in every case but further investigation is needed to determine whether these resulting currents are always of reasonable reactivity. Also, work is needed to determine whether currents corresponding to different near field measurement pattern cuts computed through this algorithm will be consistent.

Finally, the sensitivity of the current solution to increased measurement sampling distance and decreased measurement range was investigated. It was found that the sampling distance could be increased by at least a factor of 4 but no more than a factor of 8 with little change in the resultant currents. The currents, though, were highly sensitive to changes in measurement range. The trend seemed to be increased size in the invisible lobes of the free space far field plots with decreased measurement range. With extreme range curtailment the visible region of these plots also deteriorated. Correlation of the near and far region field plots corresponding to currents computed from restricted measurement range was poor. These results indicate the reason for the inconsistent unconstrained currents arise from different pattern cuts. That is, the degree of solution reactivity is associated with the amount of pattern cut energy the measurement represents.

B. CONCLUSION

The synthesis technique which requires the near field measurement of both magnitude and phase shows considerable promise as a relatively inexpensive and reliable method to determine a set of currents of an array which have corresponding radiated fields that match measurements in both the Fresnel and far field regions. It is still unknown whether the currents determined by this method are actually the currents which exist on the array. If radiation is the only concern, it is probably unimportant whether the solution obtained is actually the source distribution which exists on the array. In this case the unconstrained solution provides the best fit to the radiated fields. However if there are coupling questions involved in a problem then the reactivity of the currents is important, and the accuracy of the results rest on the degree of constraint imposed. Of course, the degree of constraint results from engineering judgement and is based on apriori knowledge of the antenna in its environment.

It appears that the synthesis technique in which only radiation magnitude data is required and in which the solution results from an iteration process is probably not practical for antenna current prediction using near field measurements. The reason lies in the fact

that the process converges only to the magnitude distribution of the measured field. The final phase distribution depends upon the initial phase assumption. Thus the resultant currents have a corresponding near field phase which may or may not match the actual near field phase. The currents, then, may or may not yield Fresnel and far field magnitude or phase patterns which correlate to those of the antenna.

Finally, it must be kept in mind that the case studied here was simple in the sense that the currents actually act as point sources for the H-plane cut considered. For arrays with more complicated elements requiring different near field pattern cuts the element current distributions become important. In this case one could apply other electromagnetic techniques to represent a more complex array element.

C. FUTURE WORK

There are some questions arising from the investigation which should be answered to acquire confidence in this process. Some less important questions concern the degree of error resulting from ideal approximations such as assuming point currents and ideal dipoles, and neglecting the array interelement and array-probe coupling. Of overriding importance, though, are thses questions related to the solution reactivity. It is necessary to determine the nature and cause of the highly reactive, inconsistent, unconstrained currents. Also, it is necessary to determine the measurement limitations necessary to guarantee accurate reproduction of the radiatiated field of the array and a reasonable solution through some constraining process. Finally, it is necessary to either verify that the algorithm presented will give reasonable consistent solutions or modify it so the problem of finding an appropriate constraint will be more straight forward.

This technique of current determination shows sufficient promise to warrant an investigation into extending it to more complicated arrays and to continuous aperture antennas. This may require a change from discrete basis vectors to continuous basis functions to aid in enforcing boundary conditions. Also, the extention of this method will require more extensive measurement techniques. Finally, the technique described in this report shows promise as an inexpensive method to find the far field pattern of an antenna array through near field measurements. Presently, the other methods commonly used to obtain far field patterns of antennas are a far field measurement and a compact range measurement. The far field measurement has the disadvantage that a large area is needed to accomplish a measurement. The compact range has the disadvantage that it is expensive. Currently, a simple compact range costs approximately a half a million dollars.

With further development, the synthesis technique described in this

report could compete with either a far field range or a compact range in the measurement of two-dimensional arrays. Also, this technique can probably be extended to antennas with continuous distributions. However, more experimental work with different antennas and more research into the theoretical aspects of the method are needed. The near field measurement device and antenna used in this study occupied 6 cubic feet and costs approximately $1500.

REFERENCES

[1] J.R. Mautz and R.F. Harrington, "Computational Methods for Antenna Pattern Synthesis," IEEE Trans. on Antennas and Propagation, Vol. AP-23, No.4, July 1975, pp. 507-512

[2] E.L. Pelton, R.J. Marhefka, and W.D. Burnside, "An Iterative Approach for Computing an Antenna Aperture Distribution from Givin Radiation Pattern Data," Technical Report 4583-6, June 1978, The Ohio State University ElectreoScience Laboratory, Department of Electrical Engineering; prepared under Contract No. N62269-76-C-0554 for Naval Air Development Center.

[3] G.A. Deschamps and H.S. Cabayan, "Antenna Synthesis and Solution of Inverse Problems by Regularization Methods," IEEE Trans. Antennas Propagat., vol AP-20, pp268-274, May 1972

[4] C.H. Walter, Traveling Wave Antennas, Dover Publications, Inc., New York, 1955, pp80-147

[5] R.E. Collin and F.J. Zucker, Antenna Theory Part 1, McGraw-Hill Book Co., New York, 1969, pp235-305

[6] D.R. Rhodes, Synthesis of Planar Antenna Sources, Oxford University Press, Oxford, 1974,pp106-127

[7] R.J. Rudduck and R.J. Marhefka, "Quasi-Optical Techniques for Antennas at UHF and Above," Quarterly Report 712242-6, Aug 1980-Oct 1980, The Ohio State University ElectroScience Laboratory, Department of Electrical Engineering; prepared under contract No. N00123-79-C-1469 for Naval Regional Procurement Office.

[8] R.C. Hanson, Geometric Theory of Diffraction, IEEE Press, New York, 1981, pp 7-21,85-98

[9] W.D. Burnside, "Analysis of On-Aircraft Antenna Patterns," Report 3390-1, Aug. 1972, The Ohio State University ElectroScience Lab., Dept of Electrical Engineering; prepared under contract N62269-72-C-0354 for Naval Air Development Center.

[10] R.J. Marhefka and W.D. Burnside, "Numerical Electromagnetic

Code(NEC)-Basic Scattering Code Part I: Users Manual," Technical Report 784508-18 Sept 1979, The Ohio State University ElectroScience Lab., Dept of Electrical Engineering; prepared under contract N00123-76-C-1371 for Naval Regional Procurement Office.

[11] F. W. Schmidt and R.J. Marhefka, "Numerical Electromagnetic Code(NEC)-Basic Scattering Code Part II: Code Manual," Technical Report 784508-14 Sept 1979, The Ohio State University ElectorScience Lab, Dept of Electrical Engineering; prepared under contract N00123-76-C-1371 for Naval Regional Procurement Office.